

Molecular Chemistry for Dark Matter

MICHAEL RYAN,^{1,2} JAMES GURIAN,^{1,3} SARAH SHANDERA,^{1,2} AND DONGHUI JEONG^{1,3}

¹*Institute for Gravitation and the Cosmos, The Pennsylvania State University, University Park, PA 16802, USA*

²*Department of Physics, The Pennsylvania State University, University Park, PA, 16802, USA*

³*Department of Astronomy and Astrophysics, The Pennsylvania State University, University Park, PA, 16802, USA*

(Dated: June 28, 2021)

ABSTRACT

Molecular cooling is essential for studying the formation of sub-structure of dissipative dark-matter halos that may host compact objects such as black holes. Here, we analyze the reaction rates relevant for the formation, dissociation, and transition of hydrogenic molecules while allowing for different values of the physical parameters: the coupling constant, the proton mass, and the electron mass. For all cases, we re-scale the reaction rates for the standard molecular hydrogen, so our results are valid as long as the dark matter is weakly coupled and one of the fermions is much heavier than the other. These results will allow a robust numerical treatment of cosmic structure, in particular for mini-halos for which molecular cooling is important, in a dissipative dark matter scenario.

Keywords: cosmology: theory – dark matter – molecular processes

1. INTRODUCTION

If the particle content of dark matter has enough complexity to support its own chemistry, the universe may contain a much richer array of structures than surveys of stars and galaxies have already revealed. Dark matter with chemistry can be dissipative, so that in sufficiently dense environments it will radiate kinetic energy and cool, allowing compact structures to form. While gravitational evidence on galactic scales indicates that any interactions among dark matter particles must be somewhat weaker than those observed in the visible matter (Markevitch et al. 2004), some small-scale data may be better explained by dark matter with self-interactions (Bullock & Boylan-Kolchin 2017). Future observations of smaller-scale structure, including the possible compact-object detections by gravitational wave obser-

vatories (Kouvaris & Tinyakov 2011; de Lavallaz & Fairbairn 2010; Bramante & Elahi 2015; Bramante & Linden 2014; Kouvaris et al. 2018; Shandera et al. 2018; Latif et al. 2019; Abbott et al. 2018, 2019; Singh et al. 2020; Hippert et al. 2021), are expected to probe the dissipative dark-matter interactions and may ultimately resolve the dark matter puzzle.

As an illustrative and calculable example, we consider a dissipative dark matter model consisting of two oppositely charged fundamental fermions with masses m and M , interacting via a $U(1)$ force mediated by a dark photon. The strength of the interaction is determined by a coupling constant, α . We take $m \ll M$ and the dark photon to be massless. For simplicity, we assume that any non-gravitational interactions between dark matter and the Standard Model particles are so weak as to be irrelevant. Here, Standard Model refers to the Standard Model of particle physics, but, hereafter, we shall use the term Standard Model for referring to atomic and molecular physics of just electrons and protons with Standard Model masses and electromagnetic interaction strength. Other dissipative scenarios, especially “mirror” dark matter where the dark sector has a copy of the particle content of the standard model, have also

mzr55@psu.edu

jhg5248@psu.edu

ses47@psu.edu

djeong@psu.edu

been studied in the literature (Berezhiani et al. 2001; Chang et al. 2019; Dessert et al. 2019; D’Amico et al. 2017; Choquette et al. 2019).

In the scenario we consider, pairs of oppositely charged particles (M and m) can form bound states analogous to hydrogen atoms, we call them *dark atoms*, and a gas of these atoms can undergo all of the familiar electromagnetic processes, including energy-level transition, ionization, and recombination. In addition to the free-free (bremsstrahlung) emission from the ionized states, dark atoms can dissipate energy by radiating dark photons through recombination or collisional excitation followed by radiative decay (Rosenberg & Fan 2017; Buckley & DiFranzo 2018). Because the neutral, bound state atoms play an important role, this dark matter model is often called “atomic” dark matter (Ackerman et al. 2009; Feng et al. 2009; Kaplan et al. 2010, 2011; Fan et al. 2013; Cyr-Racine & Sigurdson 2013; Cyr-Racine et al. 2014; Fan et al. 2013; Foot & Vagnozzi 2015; Agrawal et al. 2017; Boddy et al. 2016; Ghalsasi & McQuinn 2018).

However, the energy dissipation allowed by atomic processes requires excited-state atoms and free electrons, which are rare at low gas temperature where essentially all atoms are neutral and in the ground state. So, atomic cooling is inefficient at low temperatures. In the Standard Model, for example, cooling below 10^4 K proceeds mostly through line cooling of molecular hydrogen (Glover 2012; Mo et al. 2010). The lower-lying and more closely spaced molecular levels (see Sec. 2) allow the gas to cool to approximately 100 K. It is this low cooling temperature that determines the minimum Jeans mass for the gas fragmentation, which, in turn, sets the minimum mass of any compact objects that form from the fragments (Low & Lynden-Bell 1976; Rees 1976; Glover 2005, 2012).

The molecular and atomic cooling processes are well-studied in the Standard Model. Of particular importance to us are the atomic and molecular processes for Population III star formation that take place in a gas that is 92% hydrogen. In this paper we derive the chemical reaction rates and cooling functions relevant for the analogous processes in a gas containing all species (free particles, atoms, ions, and molecules) of “atomic” dark matter. Many of the atomic processes were derived in Rosenberg & Fan (2017), so our focus is on molecular physics.

The following three ingredients are necessary to understand the cooling processes of a gas of atoms and molecules (Flower 2007; Draine 2011): (1) the abundance of the gas comprising each species, (2) the complete set of quantum states available to each component

of the gas and how those states are populated, and (3) the interaction potentials between each species. To obtain the information from first principles requires solving multi-particle Schrödinger equations. Even within the Standard Model the solutions to these equations, and the molecular states and scattering rates, can only be found approximately and numerically. The cooling functions used in simulations of structure formation are typically semi-analytic, and significant uncertainties in various rates remain. The state of the art is reviewed, for example, in Galli & Palla (2013); Glover & Abel (2008); Glover (2015a).

Instead of obtaining the molecular wave functions, energies, and interactions from first principles, in this paper we model dark molecular processes based on the known results for Standard Model hydrogen. Fortunately, a little dimensional analysis goes a long way. For example, in the next section (Section 2), we review the Born-Oppenheimer approximation for the quantum mechanical calculation of hydrogenic molecules and show how those results can be re-scaled by ratios of the dark matter parameter values to the Standard Model values:

$$r_m = \frac{m}{511 \text{ keV}}, r_M = \frac{M}{0.938 \text{ GeV}}, r_\alpha = \frac{\alpha}{137^{-1}}. \quad (1.1)$$

We then argue that the re-scaling that we derive for the analytic but approximate Born-Oppenheimer treatment largely carries over to the more accurate but semi-analytic results used in the literature.¹ Sections 3 and 4 present the cooling functions and reaction rates obtained using these re-scaling techniques.

The result we present in this work has a broad range of potential applications including a more accurate treatment of Standard Model deuterated chemistry. However, we developed the re-scaling scheme to compute two specific aspects of dissipative dark matter scenarios: (A) the cosmological evolution of the dark molecular hydrogen fraction and (B) formation of compact objects from dark molecular cooling. We apply the outcome of this paper to these cases in two companion papers, determining the early-time makeup of the cosmological gas in Gurian & Jeong (2021) and modeling the dark-matter halo cooling from both dark hydrogen atoms and molecules in Ryan & Shandera (2021).

2. BASIC TOOLS FOR DARK MOLECULAR PHYSICS

The hydrogenic molecule is a system of two heavy particles of mass M and charge $+1$, at positions $\mathbf{X}_A, \mathbf{X}_B$,

¹ Appendix A compares our re-scaling procedure to a simpler mass re-scaling technique used in literature on Standard Model reaction rates.

and two light particles of mass m and charge -1 , at positions $\mathbf{x}_1, \mathbf{x}_2$, all interacting electromagnetically, with the fine-structure constant α . The Schrödinger equation for stationary states of this system depends on the distance between each pair of particles (e.g., x_{1A} between light particle 1 and heavy particle A) as

$$\hat{H}\Psi(\mathbf{X}_A, \mathbf{X}_B; \mathbf{x}_1, \mathbf{x}_2) = E\Psi(\mathbf{X}_A, \mathbf{X}_B; \mathbf{x}_1, \mathbf{x}_2), \quad (2.1)$$

with Hamiltonian

$$\begin{aligned} \hat{H} = & -\frac{1}{2M}(\nabla_A^2 + \nabla_B^2) - \frac{1}{2m}(\nabla_1^2 + \nabla_2^2) \\ & + \alpha \left(\frac{1}{X_{AB}} + \frac{1}{x_{12}} - \frac{1}{x_{1A}} - \frac{1}{x_{2A}} - \frac{1}{x_{1B}} - \frac{1}{x_{2B}} \right). \end{aligned} \quad (2.2)$$

Here, $\Psi(\mathbf{X}_A, \mathbf{X}_B; \mathbf{x}_1, \mathbf{x}_2)$ is the wave function for the stationary state with energy E , and we use $\hbar = 1$. We use the shorthand notation for the distance $X_{AB} \equiv |\mathbf{X}_A - \mathbf{X}_B|$, and so on. As long as $M \gg m$, we can separate the Schrödinger equation into electronic part and nucleic parts by using the Born-Oppenheimer approximation as follows. First, an ansatz for the wave functions of the light particles (the electrons) is introduced assuming the heavy particles (the protons) remain stationary (Bethe & Jackiw 1997). The electronic wave functions are only parametrically dependent on the nuclear separation X_{AB} and can be used to find an effective potential between the two nuclei, which is in turn solved for the nucleic part of the wave functions.

The simplest ansatz for the electronic ground state is the symmetric combination of products of ground state wave functions u_{is} for the individual hydrogen atoms:

$$\psi = \frac{1}{\sqrt{2}} (u_{1s}(x_{1A})u_{1s}(x_{2B}) + u_{1s}(x_{2A})u_{1s}(x_{1B})). \quad (2.3)$$

This is the Heitler-London (Heitler & London 1927) wave function for the molecule, which depends on fundamental parameters only in the usual Bohr radius combination $a_0 = (\alpha m)^{-1}$. This result is exact when the two hydrogen atoms are infinitely far apart, and provides the asymptotic form for more accurate electronic wave functions at large nuclear separation. Assuming this solution for the electronic wave functions, the effective potential for the nuclei (called the Heitler-London potential) can be written analytically. Its shape is very well approximated by the simpler Morse potential, a function of the nuclear separation:

$$V_{\text{Morse}}(X_{AB}) = V_0(e^{-2(X_{AB}-X_0)/b} - 2e^{-(X_{AB}-X_0)/b}). \quad (2.4)$$

where X_0 is the nuclear separation at the minimum of the potential, $X_0, b \propto a_0$, $V_0 \propto \alpha/a_0 \propto m\alpha^2$.

The advantage of the Morse potential is that its energy levels can be found exactly, and analytic expressions for the corresponding nuclear wave functions can be obtained (Dong 2007). The energies of the vibrational modes of the molecule are given approximately by the bound state energies in the Morse potential:

$$E_{\text{vib},\nu} = -V_0 \left(1 - \frac{\nu + \frac{1}{2}}{K_0 b} \right)^2, \quad 0 \leq \nu \leq K_0 b - \frac{1}{2}, \quad (2.5)$$

where $K_0 = \sqrt{2MV_0}$. Below the energy required to excite a vibrational mode, the separation of the two nuclei can be treated as fixed, $X_{AB} = X_0$, and then the Hamiltonian becomes that of a rigid rotor. By changing coordinates to those for the center of mass and relative motion, the usual rotational states are found with energy levels

$$E_{\text{rot},J} = \frac{J(J+1)}{MX_0^2}. \quad (2.6)$$

At this level of approximation, the molecular rotational energies and low-lying vibrational energies ($\frac{\nu}{K_0 b} \ll 1$) for generic masses $m \ll M$ and coupling ($\alpha \ll 1$) can be found from the Standard Model (SM) values via

$$\begin{aligned} E_{\text{mol. vib}} &= \left[\frac{r_\alpha^2 r_m^{3/2}}{r_M^{1/2}} \right] E_{\text{mol. vib, SM}}, \\ E_{\text{mol. rot}} &= \left[\frac{r_\alpha^2 r_m^2}{r_M} \right] E_{\text{mol. rot, SM}}. \end{aligned} \quad (2.7)$$

The literature on molecular cooling and scattering uses more accurate solutions for the molecular hydrogen energy eigenstates, found by introducing more sophisticated ansatz for the electronic wave functions. These are typically constructed from a basis set of trial wave functions, and then the task is to solve for the coefficients of the basis states that contribute to each stationary state, up to high order. For example, the James-Coolidge basis (James & Coolidge 1933) for solving the Schrödinger equation is relatively simple and is valid for small inter-nuclear distances. In this basis, the ansatz for the electronic wave functions u_{m,X_0} is written in terms of coordinates in units of the fixed nuclear separation, which up to a constant is the same as units of the Bohr radius (e.g., $y_{1A} = x_{1A}/X_0 \propto x_{1A}/a_0$):

$$\begin{aligned} u_{m,X_0} = & \sum_{\{n\}} c_{\{n\}} (1 + P_{AB})(1 + P_{12}) y_{12}^{n_1} (y_{1A} - y_{1B})^{n_2} \\ & \times (y_{2A} - y_{2B})^{n_3} (y_{1A} + y_{1B})^{n_4} (y_{2A} + y_{2B})^{n_5} \\ & \times e^{-\beta(y_{1A}+y_{1B})} e^{-\beta(y_{2A}+y_{2B})} \end{aligned} \quad (2.8)$$

where P_{AB} (P_{12}) indicates the permutation of A and B (1 and 2), and the coefficients c and β are varia-

tional parameters. The individual indices n_i are integers ≥ 0 , and the summation is over all sets of indices that satisfy $\sum_{i=1}^5 n_i \leq \Omega$ for $\Omega = 3, 4, 5, \dots$, up to the desired precision. This basis was used in [Kolos & Roothaan \(1960\)](#) in an early determination of electronic wave functions, and more recently (e.g. [Sims & Hagstrom \(2006\)](#)) to make high accuracy calculations for the hydrogen molecule. [Pachucki \(2010\)](#) gives analytic expressions for many integrals needed in molecular calculations using these wave functions. Other classic literature, beginning with a paper by [Kolos & Wolniewicz \(1965\)](#) generalizes the James-Coolidge basis to be more accurate at large distances, where it should asymptote to the Heitler-London solution. But, none of these prescriptions introduce a new parametric dependence on the fundamental parameters into the molecular potential, and so the re-scaling shown in Eq. (2.7) should remain accurate.

This can be understood as follows. Heuristically, we can obtain the re-scaling in Eq. (2.7) by using the *spring constant* for the vibrational mode

$$k = \left(\frac{d^2 V_{\text{Morse}}}{dX^2} \right)_{X=X_0} = \frac{V_0}{b^2} \propto m^3 \alpha^4, \quad (2.9)$$

and compute the vibrational energy level as

$$E_{\text{mol. vib}} = \nu \hbar \omega = \nu \hbar \sqrt{\frac{k}{M}} \propto \sqrt{\frac{m}{M}} m \alpha^2, \quad (2.10)$$

and compute the rotational energy level from moment of inertia as

$$E_{\text{mol. rot}} = \frac{L^2}{2I} \propto \frac{1}{M a_0^2} = \frac{m^2 \alpha^2}{M}. \quad (2.11)$$

Note that these heuristic results rely on the facts that the typical length scale and energy scale for the hydrogen molecule are determined by the electronic states in the framework of Born-Oppenheimer approximation. That is, it is the Bohr radius and the hydrogen binding energy that set the relevant scales, and the heuristic re-scaling must hold beyond the specific electronic wave function being used. That argument further supports our extension of the re-scaling in Eq. (2.7).

The spin part of the nuclear wave functions is also important for understanding molecular properties. There is a singlet state, parahydrogen, with total nuclear spin $S_N = 0$, and a triplet state, orthohydrogen, with total nuclear spin $S_N = 1$. Since the total wave function must be antisymmetric under the exchange of the two heavy fermions (protons) the anti-symmetric singlet state (parahydrogen) can only have J -even rotational states, while the symmetric triplet state (orthohydrogen) must have J -odd. Because the majority of radiative

transitions do not change the spin state, and a photon carries angular momentum $\Delta J = 1$, the leading order radiative transitions of hydrogenic molecules are electric quadrupole transitions, which are slower compared to the dipole transition by a factor of $(a_0/\lambda_{ul})^2$ where λ_{ul} is the wavelength corresponding to the energy gap.

2.1. Molecular binding energy

Molecular transitions and reaction rates generally depend on the ratio of the temperature to the energy scale associated with the reaction. For rotational and vibrational transitions, we presented the parametric dependence of the relevant energy scales in the previous section. On the other hand, formation and dissociation processes of molecular states involve a sum of partial cross sections over ro-vibrational states and so there is at least a formal dependence on multiple energy scales. Nonetheless, we argue that the most relevant energy scale for the formation and dissociation of hydrogenic molecules is the binding energy E_H of hydrogen.

This is most obvious in the Heitler-London treatment of the problem. Writing down the symmetric combination of ground state wave functions for the individual hydrogen atoms, Eq. (2.3) leads to an expression for the expectation value of the total energy of the molecule of the form ([Heitler & London 1927](#); [Dushman 1936](#)):

$$E_{H_2} = E_H [1 + f(X_{AB}/a_0)], \quad (2.12)$$

from which the binding energy is determined by minimizing the energy over X_{AB} and comparing to the total energy of the separated hydrogen energies. There are two key observations. First, although molecular dissociation involves separating the nuclei, the binding energy is determined principally by the electronic configuration. Second, this binding energy is (at lowest order in perturbation theory) just a constant fraction of E_H , and the constant does not depend on mass (m , M) nor coupling constant α . This method calculates a binding energy of 3.2 eV ([Heitler & London 1927](#)) compared to the measured value of 4.74 eV, and the same approach applied to H_2^+ yields an energy of 1.77 eV compared to the true value of 2.64 eV ([Li et al. 2007](#)).

Unfortunately, the accuracy of this method is clearly less than excellent. This is because the molecule is too tightly coupled for the Heitler-London wave function to be a good approximation to the molecular electronic wave function. Historically, this problem was first addressed by attaching some ansatz together with a variational parameter to the individual electron wave functions. One early such attempt is [Rosen \(1931\)](#). There, the individual electronic wave functions are given as for example

$$\psi_{1A} = u_{1s}(x_{1A}) + \sigma u'(\mathbf{x}_{1A}), \quad (2.13)$$

where u_{1s} is the hydrogenic wavefunction for an effective (screened) nuclear charge Z , and u' is the wave function of the $2p$ state in a hydrogenic atom with charge $2Z$. Both Z and σ are determined variationally. The full electronic wavefunction is taken as the Heitler-London combination of the individual electronic wavefunctions. This approach ultimately yields a ground state energy of 4.02 eV, which differs by 15.1% from the actual value, and again clearly scales as E_H .

To achieve percent-level accuracy requires a fully variational calculation, while also including the previously neglected electron-electron separation, in the James-Coolidge basis (James & Coolidge 1933) (a calculation which James & Coolidge (1933) note “can be evaluated and checked by an experienced computer in a little over two hours.”). This variational calculation may well contain some subdominant higher order energy parameter dependence which cannot be easily extracted. Still, we can be encouraged by two facts. First, the calculation is still concerned entirely with determining the electronic wave function as a function of fixed internuclear separation (and then minimizing the energy of that state with respect to the separation). Second, the variational ansatz carries dimensions only through the Bohr radius. All this makes clear that the molecular dissociation energy scales dominantly with the atomic binding energy, and that that T/E_H is the “dimensionless temperature” relevant to these reactions. Experimental data suggests that this conclusion is correct: the dissociation energy of H_2 differs from that of D_2 by less than 2% (Herzberg & Monfils 1961), consistent with predominantly E_H dependence, insensitive to the mass M .

2.2. Spontaneous emission rate

Next, we consider the spontaneous emission rates, or Einstein A coefficients. H_2 is a homonuclear molecule with no permanent electric dipole moment, so transitions between states are quadrupolar, and the hard work is to compute the quadrupole transition $\langle \Psi_{\nu, J} | \hat{Q} | \Psi_{\nu', J+2} \rangle$. Here, we bypass this calculation by re-scaling known results from the Standard Model to estimate the A coefficient for dark-atomic model.

The electric quadrupole radiation power is proportional to $P \propto \omega^6 Q^2$ (Jackson 1998), so equating that with $A^{\text{quad}} \cdot \hbar \omega$ we find the transition rate between states separated by energy ΔE scales as²

$$A^{\text{quad}} \propto \frac{\alpha(\Delta E)^5}{\hbar^5 c^4} \langle Q \rangle^2. \quad (2.14)$$

² In the literature, this rate is often given in atomic units. See Appendix B for a derivation of the re-scaling in those units.

The literature contains at least two definitions for the quadrupole moment that differ by a factor of 2 (Poll & Wolniewicz 1978; Aannestad 1973), but $Q \propto (\text{length})^2 \propto a_0^2$ regardless. In the equation above we have explicitly written the factors of \hbar so that the units on the right hand side are obviously s^{-1} .

Then, the dark matter Einstein A coefficient for transitions between rotational levels can be estimated by

$$A_{\text{rot, DM}} \propto \alpha E_{\text{mol. rot}}^5 (a_0^2)^2 \quad (2.15)$$

$$\begin{aligned} &= r_\alpha \left[\frac{r_\alpha^2 r_m^2}{r_M} \right]^5 \left(\frac{1}{(r_\alpha r_m)^2} \right)^2 A_{\text{rot, SM}} \\ &= \left[\frac{r_\alpha^7 r_m^6}{r_M^5} \right] A_{\text{rot, SM}} \end{aligned} \quad (2.16)$$

Similarly, for transitions involving only the vibrational level, we estimate the rate by

$$A_{\text{vib, DM}} \propto \alpha E_{\text{mol. vib}}^5 (a_0^2)^2 \quad (2.17)$$

$$\begin{aligned} &= r_\alpha \left[\frac{r_\alpha^2 r_m^{3/2}}{r_M^{1/2}} \right]^5 \left(\frac{1}{(r_\alpha r_m)^2} \right)^2 A_{\text{vib, SM}} \\ &= \left[\frac{r_\alpha^7 r_m^{7/2}}{r_M^{5/2}} \right] A_{\text{vib, SM}}. \end{aligned} \quad (2.18)$$

2.3. Collisional excitation scattering rates

In the simplest scattering between hydrogen molecules (H_2 - H_2), or between a hydrogen molecule and a hydrogen atom (H_2 - H), there is a change in the state of the molecule but no exchange of particles, generally called collisional excitation. Here, we discuss how to re-scale the rates for molecular scattering. We then generalize the tools developed here to general scattering processes involved in molecular chemical reactions in Section 4.

With molecular states and energies in hand from Eq. (2.7), the additional ingredient needed for scattering rates is the interaction potentials between two molecules, or between a molecule and a hydrogen atom. Takayanagi & Nishimura (1960) used a Morse-type potential in a classic analytic treatment of H_2 - H scattering. The scattering rate coefficients, $\gamma \equiv \langle \sigma v \rangle$, are determined by the velocity-averaged cross section σ for changing the rotational states, where velocity v is assumed to be drawn from a Maxwell-Boltzmann distribution at temperature T . Takayanagi & Nishimura (1960) have denoted

$$\begin{aligned} \gamma_{J, J+2} &= \langle \sigma v \rangle_{J \rightarrow J+2} \\ &= \sqrt{\frac{8}{\pi \mu k_B^3 T^3}} \int_0^\infty \sigma_{J \rightarrow J+2}(E') e^{-E'/k_B T} E' dE' \\ &= \sqrt{\frac{8k_B T}{\pi \mu}} \pi R_c^2 \langle F \rangle \end{aligned} \quad (2.19)$$

where E' is the center of mass collision energy, μ is the reduced mass of the H₂-H pair, $R_c \propto a_0$ is the distance of closest approach in a classical head-on collision. Assuming the Morse-type potential, $\langle F \rangle$ is the dimensionless result of an integral and is known analytically. Although this is a simple approach, it remains reasonably accurate even as calculations for the interaction potential have continued to improve. For example, [Wrathmall & Flower \(2007\)](#) compared a Morse-type potential, although not identical to the one used in [Takayanagi & Nishimura \(1960\)](#), to a very accurate, recent H₂-H potential and found reasonable agreement. So, we will use the Eq.(2.19) to re-scale the scattering rates.

The dimensionality of γ comes from the two factors of length in the cross section ($R_c \propto a_0$) and the thermal/kinematic factor from the velocity average, $\sqrt{k_B T/\mu}$. Since the energy difference between the initial and final levels remains parametrically important after the integration, it is useful to define the dimensionless combination $y^2 = \Delta E/(k_B T)$. While $\langle F \rangle$ is dimensionless, it does become a function of y^2 , due, at minimum, to the presence of T in the exponential term. Then, if a scattering rate is known to scale with temperature as $f(T) = f(\Delta E/y^2) = f_{\Delta E}(y)$, and using the dependence of $R_c \propto a_0$ on fundamental parameters and $\mu \propto M$, the complete parameteric dependence is

$$\gamma \propto \sqrt{\frac{\Delta E}{M}} \frac{1}{\alpha^2 m^2} f_{\Delta E}(y). \quad (2.20)$$

Collisions may cause transitions between both vibrational and rotational states in general. However, the dominant behavior of the collision can be found by treating the system approximately, separating cooling via de-excitation of rotational levels in the vibrational ground state ($\nu = 0$) which dominates at low temperatures, and cooling via transitions between the lowest few vibrational levels (averaging over the more closely spaced rotational levels), which dominates at higher temperatures.

In this approximation, we first consider transitions between rotational levels within a fixed vibrational level. Let us define the dimensionless parameter

$$y_{\text{rot}}^2 = \frac{\Delta E_{\text{rot}}}{k_B T} = \frac{m^2 \alpha^2}{M k_B T}. \quad (2.21)$$

Then, the rotational transition rate may be written as

$$\begin{aligned} \gamma &\propto \frac{1}{\alpha^2 m^2} \sqrt{\frac{\Delta E_{\text{rot}}}{M}} f_{\text{rot}}(y_{\text{rot}}) \\ &\propto \frac{1}{\alpha^2 m^2} \sqrt{\frac{\alpha^2 m^2}{M^2}} f_{\text{rot}}(y_{\text{rot}}) \\ &= \frac{f_{\text{rot}}(y_{\text{rot}})}{\alpha m M}. \end{aligned} \quad (2.22)$$

The re-scaling for the dimensionful prefactor in the dark-matter model rate coefficient is then obvious from Eq. (2.22). We can consider y_{rot}^2 as the temperature in ΔE_{rot} units, the relevant energy scale of the problem, and so both the Standard Model and dark-matter model have rotational transitions at the relevant temperatures T_{SM} and T_{DM} , with the relationship

$$T_{\text{SM}} = T_{\text{DM}} \left(\frac{\Delta E_{\text{rot,SM}}}{\Delta E_{\text{rot,DM}}} \right). \quad (2.23)$$

Using the rotational-energy re-scaling in Eq. (2.7), then, we can define a re-scaled temperature,

$$\tilde{T}_r \equiv \left(\frac{r_M}{r_m^2 r_\alpha^2} \right) T, \quad (2.24)$$

and obtain the final dark matter rate coefficient as

$$\gamma_{J,\text{DM}}(T) \approx [r_\alpha^{-1} r_m^{-1} r_M^{-1}] \gamma_{J,\text{SM}}(\tilde{T}_r). \quad (2.25)$$

The considerations for molecular-molecular scattering are more complicated than the molecular-atomic case, as the para-para, ortho-ortho, and ortho-para cases must all be considered ([McMahan et al. 1974](#); [Silvera 1980](#)). In addition, the relative orientations of the molecules is important. Still, it seems reasonable that the basic re-scaling for molecule-molecule scattering should be similar to the molecule-atom case: the cross section should increase as the size of the molecule ($R_c \propto a_0$) increases, and the reduced mass in the denominator be nearly M . We therefore use Eq. (2.25) to re-scale rates involving a change in rotational level for both H₂-H₂ and H₂-H processes.

For collisions involving a change in the vibrational level, the calculation proceeds along the same lines: the wave functions for the initial and final states are different from above, but the interaction potential is the same. So, defining

$$y_{\text{vib}}^2 = \frac{m^{3/2} \alpha^2}{M^{1/2} k_B T}, \quad (2.26)$$

assuming the collisional excitation rate similarly contains a dimensionless function that now depends on y_{vib} , $f_{\text{vib}}(y_{\text{vib}})$, and including the remaining terms from Eq. (2.20), we find that

$$\begin{aligned} \gamma_{\text{vib}} &\propto \frac{1}{\alpha^2 m^2} \sqrt{\frac{\Delta E_{\text{vib}}}{M}} f_{\text{vib}}(y_{\text{vib}}) \\ &\propto \frac{1}{\alpha^2 m^2} \sqrt{\frac{m^{3/2} \alpha^2}{M^{3/2}}} f_{\text{vib}}(y_{\text{vib}}) \\ &= \frac{f_{\text{vib}}(y_{\text{vib}})}{\alpha m^{5/4} M^{3/4}}, \end{aligned} \quad (2.27)$$

for which the re-scaling for the atomic dark-matter becomes

$$\gamma_{\text{vib,DM}}(T) \approx \left[r_\alpha^{-1} r_m^{-5/4} r_M^{-3/4} \right] \gamma_{\text{vib,SM}}(\tilde{T}_v). \quad (2.28)$$

with

$$\tilde{T}_v \equiv \left(\frac{r_M^{1/2}}{r_m^{3/2} r_\alpha^2} \right) T. \quad (2.29)$$

Again, we apply this formula for vibrational transition rates from both H₂-H₂ and H₂-H collisions.

2.4. Summary

We can extract the parametric dependence of many relevant processes in the ‘‘atomic’’ dark matter model by re-scaling only a few quantities. As we have shown, reaction and transition rates can at lowest order be treated as dependent only on some length scale (proportional to a_0) and some energy scale (atomic, rotational, or vibrational). Since H₂ has no dipole moment ($\mathbf{d} = 0$), H₂ state transitions are quadrupolar, with the vibrational and rotational Einstein coefficients derived above. We neglect higher moments, which are less important for scattering rates and cooling processes. Lastly, several reaction rates will require the ground state polarizability, a tensor mediating the external electric field and the induced electric dipole moment, $p_{ij} \propto a_0^3 \propto \frac{1}{m^3 \alpha^3}$. This is straightforward to show for the H atom (see e.g. Sakurai & Napolitano (2017) for a discussion using perturbation theory), but is more complicated for the H₂ molecule (Kolos & Wolniewicz 1967). We have listed all of the aforementioned quantities in Table 1.

3. APPLICATION: ROVIBRATIONAL COOLING FOR DARK MOLECULAR HYDROGEN

Molecular hydrogen cooling becomes important at low temperatures and high H₂ concentrations in the Standard Model (Glover 2012). In these conditions, molecular line cooling is the dominant process, with certain H₂ production and destruction channels providing auxiliary cooling. In this section, we calculate the molecular line cooling rate for the atomic dark matter model by applying the re-scaling that we have derived in Section 2.2-2.3. To start, we briefly derive the molecular line cooling equations in Sections 3.1 and 3.2, connecting our notation to that in the classic paper of Hollenbach & McKee (1979), whose analytic model forms the basis of comparison with more modern computational and empirical results (Glover & Abel 2008; Glover 2015b; Galli & Palla 1998). In Sections 3.3 and 3.4 we re-scale the equations based on the dominant physical process, and in Section 3.5 we combine the equations to obtain the full, re-scaled, rovibrational cooling rates. We present

full results based on Hollenbach & McKee (1979) as well as Glover & Abel (2008).

3.1. Molecular line cooling

Molecular line cooling occurs when the *coolant* molecules in excited states decay to lower-level states by spontaneously emitting photons. The cooling rate per volume (in units of erg s⁻¹ cm⁻³) can be written as the sum over all radiative transitions:

$$\mathcal{C} = \sum_u n_u \sum_{\ell < u} A_{u\ell} \Delta E_{u\ell}, \quad (3.1)$$

where n_u is the number density of molecules in the upper-energy state u , the ℓ are the lower-energy states available for the transition, $A_{u\ell}$ is the Einstein A coefficient, and $\Delta E_{u\ell} = E_u - E_\ell$ is the energy carried away by the photon.

Evaluating the re-scaled cooling rate from Eq. (3.1) requires knowing three pieces of information: the occupation numbers of the various rotational/vibrational levels, the re-scaled Einstein A coefficient, and the re-scaled energy of each eigenstate. We have already derived the energies in Section 2, so the energy differences are given approximately as

$$\begin{aligned} \Delta E(\nu', J \pm 2, \nu, J) \\ = (E_{\text{vib}}(\nu') - E_{\text{vib}}(\nu)) + (E_{\text{rot}}(J \pm 2) - E_{\text{rot}}(J)), \end{aligned} \quad (3.2)$$

where the vibrational and rotational energies are approximated by Eq. (2.7). We have also derived the re-scaling of the Einstein A coefficient for the electric quadrupole transition in Eqs. (2.16)-(2.18).

The remaining quantity to compute is the number density of molecules in the excited states, which depends on the temperature and the collision rate with the colliding particle X . To simplify the discussion, let us first consider the simple two-level system. If a gas is in (local) thermal equilibrium (LTE) at temperature T_{gas} , then the ratio of the population of the two states is given as the Boltzmann factor:

$$\frac{n_u^{\text{LTE}}}{n_\ell^{\text{LTE}}} = \frac{g_u}{g_\ell} \exp(-\Delta E_{u\ell}/k_B T_{\text{gas}}), \quad (3.3)$$

where $g_{u,\ell}$ are the number of internal degrees of freedom for each state. Considering those same levels as a two-state system subject to collisional excitation, collisional de-excitation, and radiative decay (without ambient radiation, or ignoring the stimulated emission or absorption), then the population of the excited state changes according to

$$\frac{dn_u}{dt} = n_X n_\ell \gamma_{\ell u} - n_X n_u \gamma_{u\ell} - n_u A_{u\ell} \quad (3.4)$$

Quantity	Dependence	Re-scaling
a_0 (Bohr radius)	$\frac{1}{\alpha m}$	$r_\alpha^{-1} r_m^{-1}$
E_H (atomic energy level spacing)	$m \alpha^2$	$r_\alpha^2 r_m$
E_{rot} (Molecular rotational energy)	$\frac{\alpha^2 m^2}{M}$	$r_\alpha^2 r_m^2 r_M^{-1}$
E_{vib} (Molecular vibrational energy)	$\frac{\alpha^2 m^{3/2}}{M^{1/2}}$	$r_\alpha^2 r_m^{3/2} r_M^{-1/2}$
\mathbf{d} (dipole moment)	0	0
A_{rot} (quadrupolar rotational Einstein coefficient)	$\frac{\alpha^7 m^6}{M^5}$	$r_\alpha^7 r_m^6 r_M^{-5}$
A_{vib} (quadrupolar vibrational Einstein coefficient)	$\frac{\alpha^7 m^{7/2}}{M^{5/2}}$	$r_\alpha^7 r_m^{7/2} r_M^{-5/2}$
p_{ij} (polarizability)	$a_0^3 = \frac{1}{m^3 \alpha^3}$	$r_\alpha^{-3} r_m^{-3}$

Table 1. Table of primary quantities important for reaction rates, their dependence on the parameters m , M , and α , and the powers of ratios of parameters (see Eq.(1.1)) needed to re-scale the quantities.

where n_X is the number density of the colliding species and $\gamma_{\ell u}$ ($\gamma_{u\ell}$) is the rate coefficient for the collisional excitation (de-excitation). The steady state solution ($dn_u/dt = 0$) is

$$\frac{n_u}{n_\ell} = \frac{n_X \gamma_{\ell u}}{n_X \gamma_{u\ell} + A_{u\ell}}. \quad (3.5)$$

There are two limiting cases. First, when the radiative decay dominates over the collisional de-excitation, ($A_{u\ell} \gg n_X \gamma_{u\ell}$), the population density in the excited states is given as $n_u = n_\ell n_X \gamma_{\ell u} / A_{u\ell}$, or the collisionally excited molecules stay in the excited states for the mean lifetime of $A_{u\ell}^{-1}$. On the other hand, when the collisional de-excitation dominates over the radiative decay, ($n_X \gamma_{u\ell} \gg A_{u\ell}$), the population at the excited state returns to the thermal solution in Eq. (3.3) because $n_u = n_\ell \gamma_{\ell u} / \gamma_{u\ell} = n_\ell g_u / g_\ell \exp(-\Delta E_{u\ell} / k_B T_{\text{gas}})$ from the principal of detailed balance. These limits are commonly denoted as the $n \rightarrow 0$ (since $n_X \ll \frac{A_{u\ell}}{\gamma_{u\ell}}$) and the LTE cases, respectively.

For a general system with more than two levels, collisional excitation, de-excitation and radiative decay can happen between any pairs of levels, so the equilibrium condition for the i -state becomes

$$\sum_{j \neq i} n_j n_X \gamma_{ji} + \sum_{j > i} n_j A_{ji} = \sum_{j \neq i} n_i n_X \gamma_{ij} + \sum_{j < i} n_i A_{ij}. \quad (3.6)$$

The three-level case can be solved analytically and solutions are given in Section 17.5 of [Draine \(2011\)](#). For systems with more than three levels, the equations are solved numerically.

As the number density of the colliding particle determines the collisional de-excitation rate, it is useful to define a critical density for level u of a collision partner X , $n_{\text{crit},u}(X)$, as a benchmark for when collisional de-excitation is important for determining the excited-level population. Although different definitions exist, the one used in [Draine](#) for example (in the limit of no ambient

radiation) is

$$n_{\text{crit},u}(X) \equiv \frac{\sum_{\ell < u} A_{u\ell}}{\sum_{\ell < u} \gamma_{u\ell}(X)}. \quad (3.7)$$

That is, this is the density of a collision particle for which collisional de-excitation equals radiative de-excitation.

The relationship between the cooling rate in Eq. (3.1) and the cooling functions L used in [Hollenbach & McKee \(1979\)](#), specific to a particular colliding particle X , is:

$$L_{u\ell}^X = \frac{1}{n(X)} \frac{1}{n(H_2)} \sum_u n_u \sum_{\ell < u} A_{u\ell} \Delta E_{u\ell} = \frac{\mathcal{C}}{n(X)n(H_2)}, \quad (3.8)$$

where L has units of $\text{erg cm}^3 \text{s}^{-1}$. Note that this definition is motivated by the fact that the upper-level population is proportional to the density of the colliding particle n_X in the low-density limit, $n_X < n_{\text{crit},u}(X)$. For example, for a simple two-level system, $\mathcal{C} = n_\ell n_X \gamma_{\ell u} \Delta E_{u\ell}$ at the low-density limit, $n_X \ll n_{\text{crit}}$, and $\mathcal{C} = n_u A_{u\ell} \Delta E_{u\ell}$ at the high-density limit, $n_X \gg n_{\text{crit}}$.

3.2. Molecular line cooling with multiple colliding particles

In the Standard Model, the main colliding particles for molecular hydrogen are atomic hydrogen and molecular hydrogen. When there is more than one colliding species then, analogous to Eq. (3.5), the steady-state population of the upper state (in the two-level approximation where we assume every pair of states separately satisfy the stationary condition) may be approximated as

$$\frac{n_u}{n_\ell} = \frac{\sum_X n_X \gamma_{\ell u}(X)}{\sum_X n_X \gamma_{u\ell}(X) + A_{u\ell}}, \quad (3.9)$$

with which the cooling rate can be written as

$$\mathcal{C} = \sum_u \sum_{\ell < u} \frac{\sum_X n_X \gamma_{\ell u}(X)}{\sum_X n_X \gamma_{u\ell}(X) + A_{u\ell}} n_\ell A_{u\ell} \Delta E_{u\ell}. \quad (3.10)$$

Let us begin by considering the two limiting cases for the density of colliding partners: the low-density and high-density limits.

When the density of colliding particles is small ($n \rightarrow 0$ limit) so that the de-excitation happens only radiatively, the cooling rate becomes,

$$\mathcal{C}_{n \rightarrow 0} \equiv \sum_X \mathcal{C}_{n \rightarrow 0}^X = \sum_X \sum_u \sum_{\ell < u} n_X n_\ell \gamma_{\ell u}(X) \Delta E_{u\ell}, \quad (3.11)$$

or every collision leads to an emission of photon with energy $\Delta E_{u\ell}$.

In the opposite ($n \rightarrow \infty$) limit, we recover the LTE cooling rate as follows. Because the H_2 molecules must be in the LTE state when the collision is frequent enough, and this must be true even with a single colliding particle species, the collisional excitation rate and the collisional de-excitation rate must satisfy individually the detailed balance relation:

$$\frac{\gamma_{\ell u}(X)}{\gamma_{u\ell}(X)} = \frac{n_u^{\text{LTE}}}{n_\ell^{\text{LTE}}} = \frac{g_u}{g_\ell} e^{-E_{u\ell}/k_B T}. \quad (3.12)$$

That means when collisional de-excitation dominates over the radiative decay,

$$A_{u\ell} \ll \sum_X n_X \gamma_{u\ell}(X), \quad (3.13)$$

we recover the LTE cooling rate

$$\begin{aligned} \mathcal{C}_{\text{LTE}} &= \sum_u n_u \sum_{\ell < u} A_{u\ell} \Delta E_{u\ell} \\ &= \frac{n(\text{H}_2)}{\mathcal{Z}} \sum_u g_u e^{-E_u/k_B T} \sum_{\ell < u} A_{u\ell} \Delta E_{u\ell}, \end{aligned} \quad (3.14)$$

where $n_u = \frac{n(\text{H}_2)}{\mathcal{Z}} g_u e^{-E_u/k_B T}$ with the partition function $\mathcal{Z} = \sum_i g_i e^{E_i/k_B T}$.

In the intermediate density regime, rather than fully solving for the level population as a function of density of all colliding particles [Eq. (3.6) or its two-level approximation in Eq. (3.9)], it is a common practice, for example in Hollenbach & McKee (1979); Galli & Palla (1998); Glover & Abel (2008), to interpolate between the low-density and high-density (LTE) cases by

$$\mathcal{C} \simeq \frac{\mathcal{C}_{\text{LTE}}}{1 + \mathcal{C}_{\text{LTE}} / \sum_X \mathcal{C}_{n \rightarrow 0}^X}, \quad (3.15)$$

so that \mathcal{C} approaches to the correct limit at both low-density and high-density limits.³

3.3. Rotational cooling rates

We must also account for the type of energy transition (rotational versus vibrational), separate from colliding particle density, since the results of Section 2 demonstrated they have different re-scalings. We first consider rotational transitions between levels J and $J-2$, in the vibrational ground state $\nu = 0$. Let $\gamma_{JJ'}^{H_2}(T)$, $\gamma_{JJ'}^{H_2}(T)$ be the rate coefficient for the ($J \rightarrow J'$) transition to occur due to a collision with, respectively, a hydrogen atom and molecule.

At the low-density ($n \rightarrow 0$) limit, with much suppressed collisional excitation, only the ground states (of both the para, $J = 0$, and ortho, $J = 1$, type molecules) are populated, and the dominant excitations are to the $J = 2$ and $J = 3$ states. Beginning with Eq. (3.1) and (3.8), we have

$$\begin{aligned} \mathcal{C}_{\text{rot}, n \rightarrow 0}^X &= n_{J=2} A_{20} \Delta E_{20} + n_{J=3} A_{31} \Delta E_{31} \\ &= n_{J=0} n(X) \gamma_{02}^X \Delta E_{20} + n_{J=1} n(X) \gamma_{13}^X \Delta E_{31} \\ &= \left(\frac{1}{4} \gamma_{02}^X \Delta E_{20} + \frac{3}{4} \gamma_{13}^X \Delta E_{31} \right) n(\text{H}_2) n(X) \\ &= \left(\frac{5}{4} \gamma_{20}^X e^{-\Delta E_{20}/k_B T} \Delta E_{20} + \frac{7}{4} \gamma_{31}^X e^{-\Delta E_{31}/k_B T} \Delta E_{31} \right) \\ &\quad \times n(\text{H}_2) n(X), \end{aligned} \quad (3.18)$$

where we use the low-density limit of Eq. (3.5), $n_u = n_\ell n(X) \gamma_{\ell u} / A_{u\ell}$, to calculate the upper-level population,

³ To understand this approximation better, let us explore the case when the approximation becomes exact. Starting from the two-level approximation in Eq. (3.10), and using Eq. (3.12), we find the cooling rate as

$$\begin{aligned} \mathcal{C} &= \sum_u \sum_{\ell < u} \frac{\sum_X n_X \gamma_{\ell u}(X)}{\sum_X n_X \gamma_{u\ell}(X) + A_{u\ell}} n_\ell A_{u\ell} \Delta E_{u\ell} \\ &= \sum_u \sum_{\ell < u} \frac{[n_u^{\text{LTE}} / n_\ell^{\text{LTE}}] n_\ell / n_u}{1 + A_{u\ell} / \sum_X [n_X \gamma_{u\ell}(X)]} n_u A_{u\ell} \Delta E_{u\ell}. \end{aligned} \quad (3.16)$$

That is, in two-level approximation, the interpolation in Eq. 3.15 is exact if the level population follows the LTE value, for which

$$\begin{aligned} \frac{A_{u\ell}}{\sum_X [n_X \gamma_{u\ell}(X)]} &= \frac{A_{u\ell} n_u \Delta E_{u\ell}}{\sum_X [n_X \gamma_{u\ell}(X) n_u \Delta E_{u\ell}]} \\ &= \frac{A_{u\ell} n_u \Delta E_{u\ell}}{\sum_X [n_X \gamma_{\ell u}(X) n_\ell \Delta E_{u\ell}]} = \frac{\mathcal{C}_{\text{LTE}}^{2\text{-level, LTE}}}{\mathcal{C}_{n \rightarrow 0}^{2\text{-level, LTE}}}. \end{aligned} \quad (3.17)$$

In reality, this approximation may work better for $T < \Delta E$ so that only a few lowest-level states are populated. This is particularly true for the rotational state where $\Delta E \propto J$, but may be little worse for the vibrational modes where the energy gap stays constant.

and set $n_{J=0}/n(\text{H}_2) = \frac{1}{4}$, $n_{J=1}/n(\text{H}_2) = \frac{3}{4}$ (i.e. ortho-para ratio of 3/1). The final equality follows from the

$$\begin{aligned}\gamma_{J,J-2}^{\text{H}}(T) &= 10^{-12} \left(\frac{10T_3^{1/2}}{1+60T_3^{-4}} + T_3 \right) \left(0.33 + 0.9 \exp \left[- \left(\frac{J-3.5}{0.9} \right)^2 \right] \right) \text{cm}^3 \text{s}^{-1} \\ \gamma_{J,J-2}^{\text{H}_2}(T) &= 3.3 \cdot 10^{-12} (1 + 2T_3) \left(0.276J^2 \exp \left[- \left(\frac{J}{3.18} \right)^{1.7} \right] \right) \text{cm}^3 \text{s}^{-1}\end{aligned}\quad (3.19)$$

where $T_3 = T/1000$ K. Because the J -dependent part in the second parenthesis is near unity for $J = 3$, we can see that $\gamma^{\text{H}_2} \gg \gamma^{\text{H}}$ for $T_3 < 1$. Hollenbach & McKee (1979) have reported that Eq. (3.19) is 50 % accurate for $0.1 < T_3 < 5$, above which we start to see the vibrational line cooling. Using our result in Eq. (2.25), the dependence on microphysical parameters can be captured by the re-scaling

$$\gamma_{J,J-2,\text{DM}}^{\text{H}(\text{H}_2)}(T) = [r_\alpha^{-1} r_m^{-1} r_M^{-1}] \gamma_{J,J-2,\text{SM}}^{\text{H}(\text{H}_2)}(\tilde{T}_r), \quad (3.20)$$

for which we evaluate the Standard Model rates at re-scaled temperature $\tilde{T}_r = r_M/r_\alpha^2 r_m^2 T$. Finally, substituting into Eq. (3.18) along with the energy re-scaling in Eq. (2.7), gives the re-scaling for the cooling rate

$$\frac{\mathcal{C}_{\text{rot},n \rightarrow 0,\text{DM}}^X(T)}{n(\text{H}_2)n(X)} = [r_\alpha r_m r_M^{-2}] \frac{\mathcal{C}_{\text{rot},n \rightarrow 0,\text{DM}}^X(\tilde{T}_r)}{n(\text{H}_2)n(X)}. \quad (3.21)$$

At the high-density limit, collisional processes dominate so that all rotational levels are in thermal equilibrium, and the cooling rate is given by Eq. (3.14):

$$\begin{aligned}\mathcal{C}_{\text{rot,LTE}}(T, n(\text{H}_2)) \\ = n(\text{H}_2) \sum_{J \geq 2} g_J \frac{\exp[-E_J/k_B T]}{\mathcal{Z}(T)} A_{J,J-2} \Delta E_{J,J-2}.\end{aligned}\quad (3.22)$$

The re-scaling results from Section 2 for the Einstein A coefficient [Eq. (2.16)] and the energy levels [Eq. (2.7)] can be used to determine the re-scaled cooling rate in the LTE regime to account for changes in the microphysical parameters as following:

$$\mathcal{C}_{\text{rot,LTE,DM}}(T) = [r_\alpha^9 r_m^8 r_M^{-6}] \mathcal{C}_{\text{rot,LTE,SM}}(\tilde{T}_r). \quad (3.23)$$

We then calculate the cooling rate in the intermediate density regime by interpolation following Eq. (3.15).

detailed-balance relation in Eq. (3.12). The total cooling rate is given as the sum $\mathcal{C} = \sum_{X=\text{H},\text{H}_2} \mathcal{C}^X$.

Hollenbach & McKee (1979) provide an analytic form for a fit to the low-density limit collisional de-excitation rates

3.4. Vibrational cooling rates

For cooling by vibrational transitions, we follow Hollenbach & McKee (1979) who approximate the states as a three-level system ($\nu = 2, 1, 0$), assuming all levels have the same number of internal degrees of freedom ($g_0 = g_1 = g_2 = 1$). We also follow them in approximating the vibrational motion as the simple harmonic oscillator, so that the energy levels are proportional to ν (dropping the terms higher order in ν): $\Delta E_{10} = \Delta E_{21} = 0.5 \Delta E_{20}$. Because the rotational energy gap is much smaller than the vibrational gap, we ignore any differences in energy if the J value changes in the transition.

The low-density limit for this system comes from a similar calculation as was used above for the rotational case, except that the factor from degrees of freedom is one (compared to $(2J+1)/(2J-3)$) and there is no distinction between para and ortho states:

$$\begin{aligned}\frac{\mathcal{C}_{\text{vib},n \rightarrow 0}^X}{n(\text{H}_2)n(X)\Delta E_{10}} \\ = \gamma_{10}^X e^{-\Delta E_{10}/k_B T} + 2\gamma_{20}^X e^{-\Delta E_{20}/k_B T} + \gamma_{21}^X e^{-\Delta E_{21}/k_B T},\end{aligned}\quad (3.24)$$

which is nearly the expression given by Hollenbach & McKee (1979) except that we have included the γ_{21} term dropped there. The expression including the γ_{21} term provides a better fit to the later results of Glover & Abel (2008). As for the collisional de-excitation rates, we use

Hollenbach & McKee (1979)⁴:

$$\gamma_{10}^{\text{H}} = 1.0 \cdot 10^{-12} T^{1/2} \exp\left[-\frac{1000}{T}\right] \text{ cm}^3/\text{s} \quad (3.25)$$

$$\gamma_{20}^{\text{H}} = 1.6 \cdot 10^{-12} T^{1/2} \exp\left[-\left(\frac{400}{T}\right)^2\right] \text{ cm}^3/\text{s} \quad (3.26)$$

$$\gamma_{21}^{\text{H}} = 4.5 \cdot 10^{-12} T^{1/2} \exp\left[-\left(\frac{500}{T}\right)^2\right] \text{ cm}^3/\text{s} \quad (3.27)$$

$$\gamma_{10}^{\text{H}_2} = 1.4 \cdot 10^{-12} T^{1/2} \exp\left(-\frac{12000}{T+1200}\right) \text{ cm}^3/\text{s} \quad (3.28)$$

$$\gamma_{21}^{\text{H}_2} = \gamma_{10}^{\text{H}_2} \quad (3.29)$$

$$\gamma_{20}^{\text{H}_2} = 0 \quad (3.30)$$

where T is in unit of K , then re-scale these rates by using Eq. (2.28):

$$\gamma_{\text{vib,DM}}^X(T) \approx \left[r_\alpha^{-1} r_m^{-5/4} r_M^{-3/4}\right] \gamma_{\text{vib,SM}}^X(\tilde{T}_v), \quad (3.31)$$

with $\tilde{T}_v \equiv \left(\frac{r_M^{1/2}}{r_m^{3/2} r_\alpha}\right) T$. Finally, substituting into

Eq. (3.18) along with the energy re-scaling in Eq. (2.7), gives the re-scaling for the cooling rate

$$\frac{\mathcal{C}_{\text{vib},n \rightarrow 0, \text{DM}}^X(T)}{n(\text{H}_2)n(X)} = \left[r_\alpha r_m^{1/4} r_M^{-5/4}\right] \frac{\mathcal{C}_{\text{vib},n \rightarrow 0, \text{DM}}^X(\tilde{T}_v)}{n(\text{H}_2)n(X)}. \quad (3.32)$$

At the high-density limit, collisional processes dominate so that all vibrational levels are in thermal equilibrium, and the cooling rate is given by Eq. (3.14):

$$\begin{aligned} \mathcal{C}_{\text{vib,LTE}}(T, n(\text{H}_2)) & \quad (3.33) \\ = n(\text{H}_2) \sum_{\nu, \nu' < \nu} g_J \frac{\exp[-E_\nu/k_B T]}{\mathcal{Z}(T)} A_{\nu\nu'} \Delta E_{\nu\nu'} \end{aligned}$$

From the re-scaling results from Section 2 for the Einstein A coefficient [Eq. (2.18)] and the energy levels [Eq. (2.7)], we find the re-scaled cooling rate in the LTE regime:

$$\mathcal{C}_{\text{vib,LTE,DM}}(T) = \left[r_\alpha^9 r_m^5 r_M^{-3}\right] \mathcal{C}_{\text{vib,LTE,SM}}(\tilde{T}_v). \quad (3.34)$$

3.5. Rovibrational cooling

To calculate the total cooling rate, we have to combine the rotational cooling rate and vibrational cooling rate.

⁴ Although the $\gamma_{21}^{\text{H}_2} = \gamma_{10}^{\text{H}_2}$ rate coefficients have been updated in Hollenbach & McKee (1989), we use the original here and in Figures 1 and 2 for simplicity, since the change amounts to a net decrease by a factor of at most two in a small temperature region.

First of all, using the approximation in Eq. (3.15), we can combine the results of the previous sections by

$$\begin{aligned} \mathcal{C}_{\text{tot}} &= \mathcal{C}_{\text{rot}} + \mathcal{C}_{\text{vib}} \\ &= \frac{\mathcal{C}_{\text{rot,LTE}}}{1 + \mathcal{C}_{\text{rot,LTE}}/\sum_X \mathcal{C}_{\text{rot},n \rightarrow 0}^X} \\ &\quad + \frac{\mathcal{C}_{\text{vib,LTE}}}{1 + \mathcal{C}_{\text{vib,LTE}}/\sum_X \mathcal{C}_{\text{vib},n \rightarrow 0}^X}, \end{aligned} \quad (3.35)$$

with $X = \text{H}, \text{H}_2$ being the colliding particles. As described in the previous sections, we use the collisional excitation rates from Hollenbach & McKee (1979).

On the other hand, most recent literature combines the rotational and vibrational cooling rates in the manner specified in Galli & Palla (1998)

$$\mathcal{C}_{\text{tot}} = \frac{\mathcal{C}_{\text{rot,LTE}} + \mathcal{C}_{\text{vib,LTE}}}{1 + (\mathcal{C}_{\text{rot,LTE}} + \mathcal{C}_{\text{vib,LTE}})/\mathcal{C}_{\text{tot},n \rightarrow 0}}, \quad (3.36)$$

with

$$\mathcal{C}_{\text{tot},n \rightarrow 0} = \sum_X (\mathcal{C}_{\text{rot},n \rightarrow 0}^X + \mathcal{C}_{\text{vib},n \rightarrow 0}^X). \quad (3.37)$$

Since more recent rates have improved collisional coefficients (Galli & Palla 1998), and include ortho-para conversions and other improvements (Glover & Abel 2008), we would prefer to use the rate formulation given in Eq. (3.36). This introduces complications, however, as the low-density limit terms $\mathcal{C}_{\text{rot},n \rightarrow 0}^{\text{H}, \text{H}_2}$ and $\mathcal{C}_{\text{vib},n \rightarrow 0}^{\text{H}, \text{H}_2}$ are usually given in the form of an analytic fit to the sum $\mathcal{C}_{\text{rot},n \rightarrow 0}^{\text{H}, \text{H}_2} + \mathcal{C}_{\text{vib},n \rightarrow 0}^{\text{H}, \text{H}_2}$, while the LTE terms are generally given individually. This poses a non-trivial problem for our purpose, because, as demonstrated in Sections 3.3 and 3.4, rotational and vibrational processes are subject to different re-scalings. In Appendix C, we present a method for re-scaling the total cooling rate with the assumption that rotational cooling rate and vibrational cooling rate dominate at opposite ends of the temperature range.

In Figure 1, we show the resulting low-density-limit total cooling rate of the hydrogenic molecule colliding with H or H₂. For literature comparison, we have plotted Λ defined as

$$\Lambda^X = \frac{\mathcal{C}_{\text{rot},n \rightarrow 0}^X + \mathcal{C}_{\text{vib},n \rightarrow 0}^X}{(n(\text{H}) + n(p) + 2n(\text{H}_2))^2}. \quad (3.38)$$

For this plot, we choose the values $n(\text{H}_2) = 10^{-4} \text{ cm}^{-3}$, $n(\text{H}) = 1 \text{ cm}^{-3}$, and neglect the ionized state $n(p)$. While simply using just the rotational or just the vibrational re-scaling is insufficient (*top-right* panel), the method that we outlined in Appendix C provides results close to what we obtain by re-scaling the individual rotational and vibrational formulas in Hollenbach

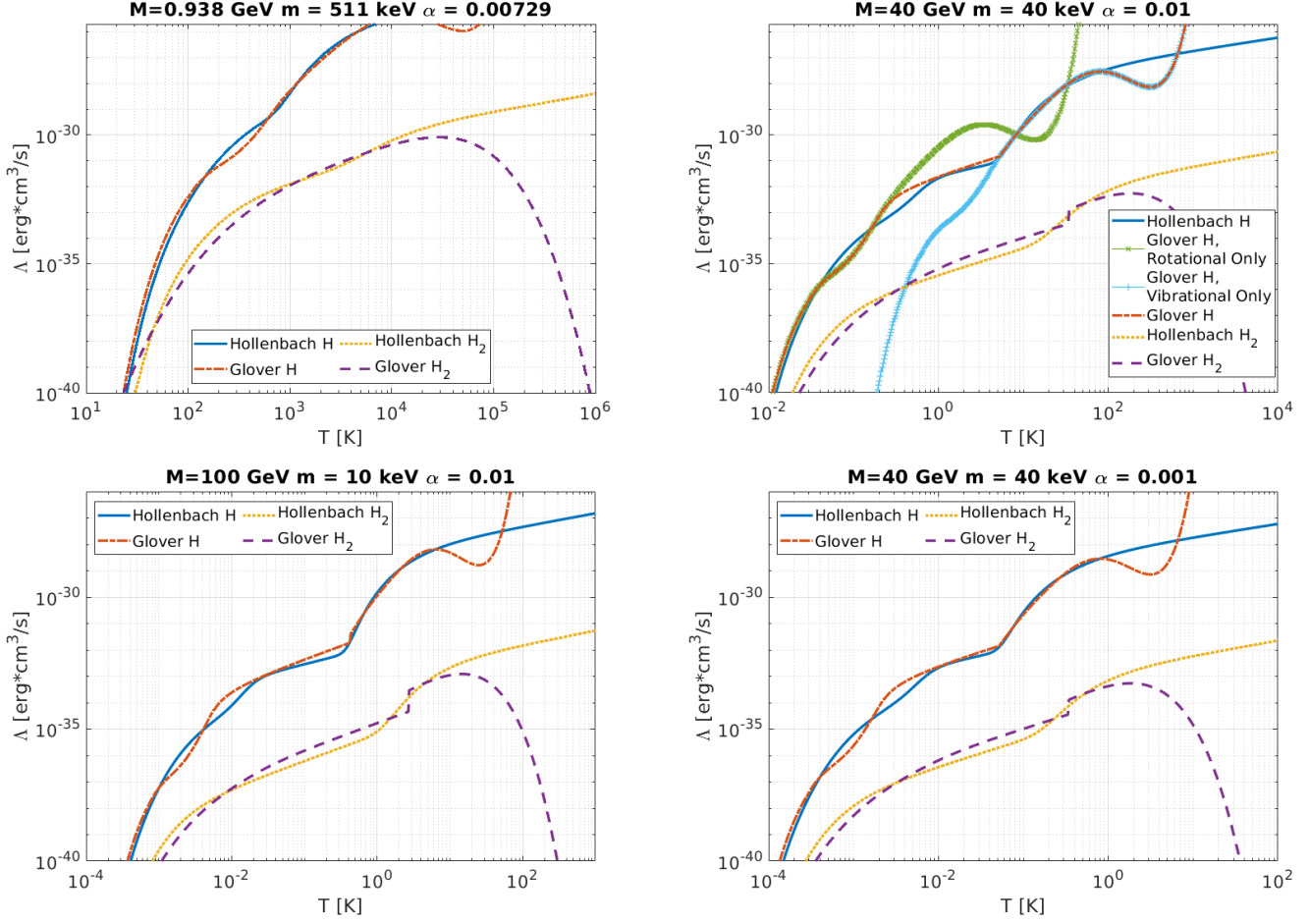


Figure 1. $\text{H}_2 - \{\text{H}, \text{H}_2\}$ collisional cooling curves obtained from Hollenbach & McKee (1979) and Glover & Abel (2008) in the low-density limit ($\Lambda_{n \rightarrow 0}^{\text{H}, \text{H}_2}$). All plots have $n(\text{H}_2) = 10^{-4} \text{ cm}^{-3}$ and $n(\text{H}) = 1 \text{ cm}^{-3}$. The **top left** panel shows a comparison of two cooling curves with Standard Model values. The **top right** panel demonstrates the necessity of including both rotational and vibrational re-scaling for atomic dark matter parameters $(M, m, \alpha) = (40 \text{ GeV}, 40 \text{ keV}, 0.01)$: the Glover curves are shown using rotational only (green x), vibrational only (cyan +), or both rotational and vibrational re-scaling (red dash-dot). Clearly, using only one re-scaling fails in temperature regions with a different dominant process. The lower Hollenbach and McKee curves in the upper left plot, and all curves in the lower two plots, use the combined re-scaling detailed in Appendix C. The “kink” in the H_2 curves arises from a combination of approximating the H_2 transition temperature re-scaling and the simple gap-filling method we use. The other parameter values shown are $(M, m, \alpha) = (100 \text{ GeV}, 10 \text{ keV}, 0.01)$ (**bottom left**), and $(M, m, \alpha) = (40 \text{ GeV}, 40 \text{ keV}, 0.001)$ (**bottom right**).

& McKee (1979) (and outlined in the previous section). This method, therefore, allows us to re-scale the modern and more accurate cooling function from Glover & Abel (2008). Note that the fit from Glover & Abel (2008) is only well-defined in the range $10 \text{ K} \leq T \leq 10^4 \text{ K}$, as can be seen by the high temperature divergences in the Standard Model (*top-left* panel), and that this range shifts proportionally to the dark parameters. The high temperature divergences are not a significant issue, however, as they occur above the disassociation temperature, 4.48 eV; hence, we do not expect to have significant amounts of hydrogen molecules at that temperature.

Finally, in Figure 2, we show the entire “atomic” dark matter cooling rate Λ including both the molecular rovi-

brational cooling defined above and the combination of cooling processes provided in Rosenberg & Fan (2017). We have computed the rate for the same dark parameter sets used in Figure 1 to demonstrate the significant behavioral changes induced by varying the parameters. We have also varied the ionization fraction and the dark-atomic hydrogen fractions x_{H_2} to match the cosmological abundance obtained in Gurian & Jeong (2021).

4. APPLICATION: REACTION RATES

The molecular line cooling in the previous section is proportional to the abundance of H and H_2 . In order to complete the molecular line cooling calculation for the dark-atomic model, therefore, we have to determine

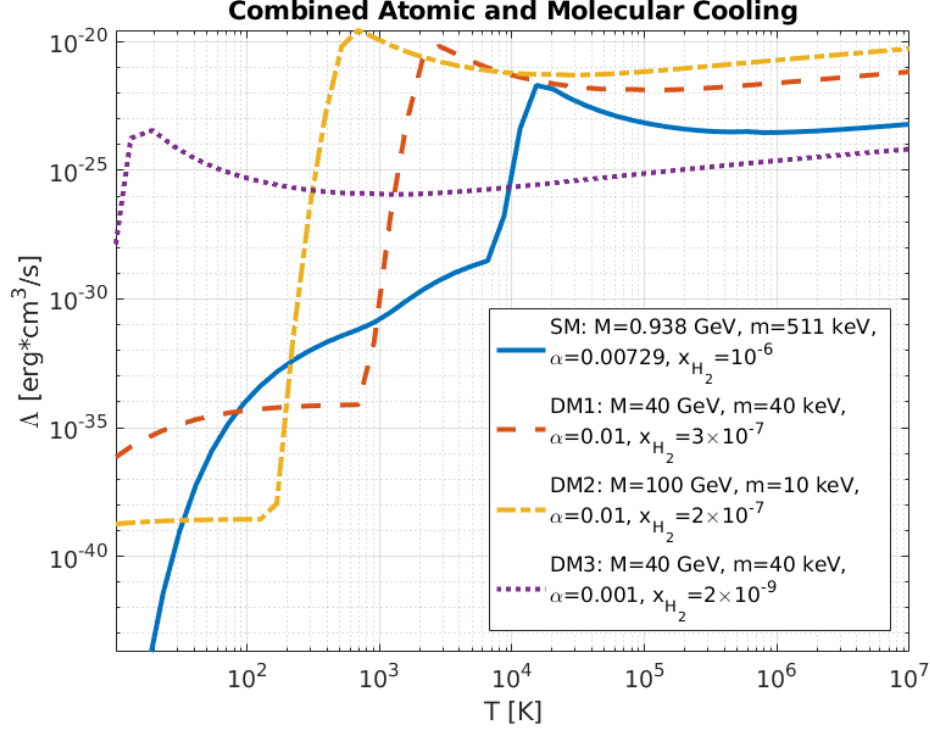


Figure 2. Combined atomic and molecular cooling rate for “atomic” dark matter for the dark parameters listed. The atomic cooling rates were derived in [Rosenberg & Fan \(2017\)](#) and the H_2 fraction, x_{H_2} , represents the cosmological fraction found in [Gurian & Jeong \(2021\)](#). Note that the molecular cooling can be significantly reduced compared to atomic cooling as the parameters are varied from the Standard Model values.

their abundances. These abundances are generally computed numerically from a set of coupled differential rate equations similar to Eq. (3.4), for example,

$$\frac{dn_{\text{H}_2}}{dt} = \sum_{j \in F_i} \left(\gamma_j \prod_{k \in R_j} n_k \right) - \sum_{j \in D_i} \left(\gamma_j \prod_{k \in R_j} n_k \right), \quad (4.1)$$

where the first sum represents the source term including all chemical reactions that contain H_2 as one of the products (Formation reactions), and the second sum represents the sink term including all chemical reactions that contain H_2 as one of the reactants (Destruction reactions). Thus, to determine the species’ abundance evolution in the atomic dark matter model, we need to know how to re-scale the reaction rates (γ) to give the leading dependence on the dark-matter parameters, the main topic of this section. In the first sub-section, we give an overview of how the re-scaling procedure works and present a summary table of our results. In the remaining sub-sections we provide the details.

4.1. Overview of method and summary of result

Just like the case for the collisional excitation rates that we studied in Section 2.3, from a given standard model rate γ_{SM} , the corresponding rate for the dark

matter model can be estimated by an overall re-scaling factor multiplying γ_{SM} evaluated at a re-scaled temperature \tilde{T} . That is,

$$\gamma_{\text{DM}}(T) = g(r_\alpha, r_m, r_M) \gamma_{\text{SM}}(\tilde{T}_\Delta), \quad (4.2)$$

where $g(r_\alpha, r_m, r_M)$ is the overall re-scaling, and $\tilde{T}_\Delta = T/r_{\Delta E}$ with $r_{\Delta E}$ the re-scaling of the primary binding energy relevant for the reaction.

For non-photochemistry reactions, the calculations of interaction rates are similar to Eq. (2.19) from Section 2, but with the added possibility of chemical reactions instead of just pure scattering. Assuming that all particles in the gas are at the same temperature, the reaction rate is

$$\gamma_{\text{DM,non-}\gamma} = \langle \sigma v \rangle \propto \sqrt{\frac{T}{\mu}} \int_0^\infty \sigma(x; y) x^3 e^{-x^2} dx. \quad (4.3)$$

Here, we reuse the two dimensionless parameters defined in Section 2:

$$x^2 = \frac{\text{K.E.}}{k_B T} = \frac{\mu v^2}{2 k_B T}, \quad (4.4)$$

$$y^2 = \frac{\Delta E}{k_B T}, \quad (4.5)$$

where ΔE is the relevant binding energy of the chemical reactions. Note that, for chemical reactions, we cannot assume that the cross-section scales only as some effective size of the particles. Instead, we need to determine in more detail how the cross section depends on kinetic energy and binding energies, and how strongly the reaction depends on α .

Even for chemical reactions, however, we can organize the scattering rate, Eq. (4.3), as a product of the universal thermal factor, an effective ‘‘impact parameter’’ \tilde{R} (with dimensions of length) squared, and a dimensionless integral, analogously to Eq. (2.19). The reaction-dependent part of the pre-factor, $g(r_\alpha, r_m, r_M)$, then depends on the re-scaling of the ‘‘impact parameter’’. In general, this will be an algebraic combination of the masses, α , and T (we do not need to track whether the T comes from x or y substitutions). Considering only the dominant parametric dependence as power laws, the pre-factor can be written

$$g(r_\alpha, r_m, r_M) = \left(r_\mu^{-1/2} r_{\Delta E}^{1/2} \right) \left(r_\alpha^{R_\alpha} r_m^{R_m} r_M^{R_M} r_{\Delta E}^{R_T} \right), \quad (4.6)$$

where the terms in the first parenthesis come from the universal thermal factor, and the terms in the second are from the parametric dependencies of \tilde{R} .

For photochemistry reactions, we have different factors and integrals, but the overall approach is identical, with the substitution of the radiation temperature, T_γ , instead of the particle temperature, T , and a slightly different universal thermal factor. Thus, we have

$$\begin{aligned} \gamma_{\text{DM},\gamma}(T_\gamma) &= 2c \int_{\Delta E/h}^{\infty} d\nu \frac{\nu^2 \sigma_{\text{photo}}(\nu)}{e^{h\nu/k_B T_\gamma} - 1} \\ &= g(r_\alpha, r_m, r_M) \gamma_{\text{SM},\gamma} \left(\frac{T_\gamma}{r_{\Delta E}} \right), \end{aligned} \quad (4.7)$$

with

$$g(r_\alpha, r_m, r_M) = \left(r_{\Delta E}^3 \right) \left(r_\alpha^{R_\alpha} r_m^{R_m} r_M^{R_M} r_{\Delta E}^{R_T} \right). \quad (4.8)$$

Table 2 summarizes the main results of this section. This table contains only ‘‘the most important’’ molecular hydrogen reactions as designated by Galli & Palla (1998) (see also Abel et al. (1997)). These reactions are required for calculating the abundance of dark-molecular hydrogen and used in Gurian & Jeong (2021); Ryan & Shandera (2021). The table shows the parametric dependence of the cross sections, the re-scaling pre-factor (capturing only the dominant parametric dependence), and the dominant power-law temperature dependence of the rate as b . Standard Model rates frequently have a temperature dependence that can be captured to a first approximation by a power law $\gamma_{\text{SM}} \propto T^b$,

and it is often useful to see this power law in order to understand the primary parametric dependence of a reaction. However, the full temperature dependence known for the Standard Model can of course be used (as long as the re-scaled temperature is used throughout) and is recommended. In the following sub-sections we go through detailed derivations of a few representative cases.

Principle of detailed balance—Several reactions in Table 2 are inverses of each other, and we can exploit that property to compute some re-scalings using the principal of detailed balance (Mo et al. 2010). In thermal equilibrium, forward and backward reaction rates must match, leading to the following relationship between their cross sections:

$$\sigma_f \propto \left(\frac{g_b}{g_f} \right) \left(\frac{p_b}{p_f} \right)^2 \sigma_b, \quad (4.9)$$

While p_b and p_f are reaction specific, recombination/photoionization-type reactions all have $p_b = \frac{h\nu}{c}$ and $p_f = m_{\text{ej}} v$ and we obtain the Milne Relation (Mo et al. 2010),

$$\sigma_{\text{rec}}(v, n) = \frac{g_n}{g_{n+1}} \left(\frac{h\nu}{m_{\text{ej}} v c} \right)^2 \sigma_{\text{pi}}(\nu, n), \quad (4.10)$$

where σ_{rec} is the recombination cross section, σ_{pi} is the photonionization cross section, $h\nu$ is the photon energy, and $m_{\text{ej}} v$ is the momentum of the ejected particle (e.g. an electron in standard hydrogen recombination; see Section 4.2). Generally, we have $h\nu = \text{K.E.} + \Delta E = k_B T (x^2 + y^2)$ through conservation of energy (with x and y defined in Eqs. (4.4) - (4.5)) and usually $m_{\text{ej}} \approx \mu$, such that

$$\sigma_{\text{rec}} \propto \frac{T}{\mu} \frac{(x^2 + y^2)^2}{x^2} \sigma_{\text{pi}} \quad (4.11)$$

4.2. Reaction 1: Hydrogen recombination

Let us start with one of the simplest reactions, hydrogen recombination: $p + e \rightarrow \text{H} + \gamma$. This reaction is often divided into Case A, where the hydrogen atoms are sparse enough to recombine directly to the ground state, and Case B, where the hydrogen atoms are too dense for the Lyman-series photons to escape, restricting recombination to excited states. The dependence on dark-sector parameters has been worked out already in Rosenberg & Fan (2017) (Case A) and in Hart & Chluba (2017) (Case B), and so this is a good example to demonstrate the validity of the re-scaling procedure in this work. Both Case A and Case B scenarios have no impact on the re-scaling of the cross section, but the reaction rates do of course differ. In Table 2, we have used b values derived from the Case B rate of Pequignot et al. (1991) in order to have a relevant comparison to

Reaction	Cross Section Source	σ	Re-scaling Pre-factor $g(r_\alpha, r_m, r_M)$	b	Additional Notes
1 $p + e \rightarrow H + \gamma$ (4.2)	Mo et al. (2010)	$\frac{\alpha^5}{K_E(K_E + \Delta E)}$	$r_\alpha^2 r_m^{-2}$	-0.62, -1.15	1,2
2 $H + \gamma \rightarrow p + e$ (4.2)	Mo et al. (2010)	$\mu \alpha^5 \frac{1}{(K_E + \Delta E)^3}$	$r_\alpha^5 r_m$	0.88, 0.35	3
3 $H + e \rightarrow H^- + \gamma$ (4.3)	de Jong (1972)	$\frac{\alpha}{\mu^2} \frac{\Delta E^{1/2} K_E^{1/2}}{(K_E + \Delta E)}$	$r_\alpha^2 r_m^{-2}$	0.928	1,4
4 $H^- + \gamma \rightarrow H_D + e$	Armstrong (1963)	$\frac{\alpha}{\mu} \frac{\Delta E^{1/2} K^{3/2}}{(K_E + \Delta E)^3}$	$r_\alpha^5 r_m$	2.13	3,4
5 $H^- + H \rightarrow H_2 + e$	Browne & Dalgarno (1969)	$\sqrt{\frac{\alpha \alpha_0^3}{K_E}}$	$r_\alpha^{-1} r_m^{-3/2} r_M^{-1/2}$	0	5,6,7
7 $H^- + p \rightarrow 2H$ (4.4)	Bates & Lewis (1955)	$\alpha \alpha_0^2 \sqrt{\mu} \frac{\sqrt{K_E + \Delta E}}{K_E \Delta E}$	$r_\alpha^{-3} r_m^{-3}$	$-\frac{1}{2}$	5,8
8 $H + p \rightarrow H_2^+ + \gamma$	Stancil et al. (1993)	$\frac{\alpha}{E_H^3} \frac{K_E \cdot 3/2 M^{1/2}}{(K_E + \Delta E)^3 \alpha^4}$	$r_\alpha^2 r_m^{-1} r_M^{-1}$	1.8	9
9 $H_2^+ + \gamma \rightarrow H + p$	Stancil et al. (1993)	$(\frac{\mu \nu}{h \nu})^2 \frac{(K_E + \Delta E)^3 \alpha^4}{E_H^3 K_E \cdot 3/2 M^{1/2}}$	$r_\alpha^5 r_m^{-1/2} r_M$	1.59	3,10
10 $H_2^+ + H \rightarrow H_2 + p$ (4.5)	Galli & Palla (1998)	$\sqrt{\frac{\alpha \alpha_0^3}{K_E}}$	$r_\alpha^{-1} r_m^{-3/2} r_M^{-1/2}$	0	7
15 $H_2 + p \rightarrow H_2^+ + H$ (4.5)	Galli & Palla (1998)	$\sqrt{\frac{\alpha \alpha_0^3}{K_E}}$	$r_\alpha^{-1} r_m^{-3/2} r_M^{-1/2}$	0	7,10
18 $H_2 + \gamma \rightarrow H_2^+ + e$	ONeil & Reinhardt (1978)	$\alpha \alpha_0^5 (K_E + \Delta E)$	$r_\alpha^4 r_m^{-1}$	1.56	3

Table 2. Table of Reactions. Reactions are numbered according to Galli & Palla (1998) and the section numbers in parentheses indicate where details can be found in the text. Only the parametric dependence on key quantities are shown for the cross sections (no numerical factors). The reactions included in this table are only those that were considered “important” in Galli & Palla (1998) or that are required for our companion paper (Curian & Jeong 2021). To leading order the Standard Model rates can be approximated as $\gamma \propto g(r_\alpha, r_m, r_M) (T/r_{\Delta E})^b$ and values for b are from Galli and Palla unless otherwise noted. All reactions listed have binding energy proportional to E_H , so here $r_{\Delta E} = r_\alpha^2 r_m$. For reactions 1-4 and 18, the reduced mass, μ , is proportional to the dark electron mass, m . For the remaining reactions, μ is proportional to the dark proton mass, M .

¹ Milne Relation ² The b values are an expansion of the Case B recombination coefficient in low and high temperature regimes (respectively), from Pequignot et al. (1991). The re-scaling of the Case A coefficient is identical, although b differs. ³ Photoionization re-scaling ⁴ Effective Range approximation ⁵ These rates are uncertain by up to an order of magnitude Glover & Abel (2008) ⁶ Rate is constant for $T < 300$ K, and very uncertain for $T > 300$ K Galli & Palla (1998) ⁷ Langevin Reaction ⁸ Landau-Zener method ⁹ b value from Stancil et al. (1998) ¹⁰ General Detailed Balance

the photoionization rate, which does not contribute to ionizing photons when the medium is optically thin. In this section, we obtain the expression for the recombination cross-section using the principal of detailed balance and the photoionization cross section, and apply this expression to the Case A rate of Cen (1992).

The photoionization cross section from the ground state of a hydrogenic atom is (Mo et al. 2010)

$$\sigma_{\text{pi}}(\nu) = \frac{g_{\text{bf}}}{Z^2} \frac{64\pi}{3\sqrt{3}} \frac{h^2}{\alpha m^2 c^2} \left[\frac{E_{\text{H}}}{h\nu} \right]^3 \propto \alpha a_0^2 \left(\frac{E_{\text{H}}}{h\nu} \right)^3, \quad (4.12)$$

where $E_{\text{H}} = \frac{\alpha}{2a_0}$ is the binding energy of hydrogen, g_{bf} is the bound-free Gaunt factor, and Z is the nuclear charge ($Z = 1$ in the “atomic” dark matter case). From conservation of energy, $h\nu = \text{K.E.} + \Delta E$, and we have

$$\sigma_{\text{pi}} \propto \alpha a_0^2 \frac{\left(\frac{\alpha}{a_0}\right)^3}{(\text{K.E.} + \Delta E)^3} = m \alpha^5 \frac{1}{(k_B T(x^2 + y^2))^3}. \quad (4.13)$$

Now that we have the photoionization cross section, application of the Milne relation [Eq. (4.10)] with $\mu = m$ gives

$$\sigma_{\text{rec}} \propto \left(\frac{\alpha^5}{T^2} \right) \left(\frac{1}{x^2(x^2 + y^2)} \right). \quad (4.14)$$

Substituting this into Eq. (4.6) and defining $\tilde{T}_a = T/(r_\alpha^2 r_m)$ as the atomic energy analog of \tilde{T}_r and \tilde{T}_v , we obtain our final re-scaling

$$\gamma_{\text{rec,DM}}(T) = [r_\alpha^2 r_m^{-2}] \gamma_{\text{rec,SM}}(\tilde{T}_a). \quad (4.15)$$

which matches the results in Rosenberg & Fan (2017) and Hart & Chluba (2017).

A simplified Standard Model recombination rate is given by Cen (1992); Mo et al. (2010):

$$\gamma_{\text{rec,SM}}(T) = 8.40 \times 10^{-11} \text{ cm}^3 \text{ s}^{-1} T^{-1/2} \left(\frac{T}{10^3 \text{ K}} \right)^{-0.2} \left(1 + \left(\frac{T}{10^6 \text{ K}} \right)^{0.7} \right)^{-1}, \quad (4.16)$$

and we find the corresponding dark recombination rate following the procedure in Section 4.1 as

$$\begin{aligned} \gamma_{\text{rec,DM}}(T) &= 2.66 \times 10^{-12} \text{ cm}^3 \text{ s}^{-1} [r_\alpha^2 r_m^{-2}] \left(\frac{T/(r_\alpha^2 r_m)}{10^3 \text{ K}} \right)^{-0.7} \left(1 + \left(\frac{T/(r_\alpha^2 r_m)}{10^6 \text{ K}} \right)^{0.7} \right)^{-1} \\ &\approx \left\{ \begin{array}{ll} 2.66 \times 10^{-12} [r_\alpha^{3.4} r_m^{-1.3}] \left(\frac{T}{10^3 \text{ K}} \right)^{-0.7} & T \ll r_\alpha^2 r_m 10^6 \text{ K} \\ 2.11 \times 10^{-14} [r_\alpha^{4.8} r_m^{-0.6}] \left(\frac{T}{10^6 \text{ K}} \right)^{-1.4} & T \gg r_\alpha^2 r_m 10^6 \text{ K} \end{array} \right\} \text{ cm}^3 \text{ s}^{-1} \end{aligned} \quad (4.17)$$

In Figure 3, we show that this re-scaling provides a good approximation of the true dark recombination rate and that we can improve on these results simply by using the same re-scaling but a more accurate Standard Model rate with the form,

$$\gamma_{\text{rec,SM}}(T) = \exp \left(\sum_{n=0}^9 A_n \log(T)^n \right), \quad (4.18)$$

where the coefficients are given in Abel et al. (1997). We compare the re-scaled recombination rates, Eq. (4.17) and the re-scaled version of Eq. (4.18) with the first-principle calculation from Rosenberg & Fan (2017) in Fig. 3.

4.3. Reaction 3 and 4: Hydrogen electron attachment and H^- photodetachment

The hydrogen electron attachment reaction, $\text{H} + e^- \rightarrow \text{H}^- + \gamma$, can be effectively treated as a screened proton capturing a free electron, in a similar process to standard hydrogen recombination (Ohmura & Ohmura 1960). The reaction rate can be computed in analogous fashion, but where the H^- photodetachment cross section is used instead of the H photoionization cross section. Thus, we start with the photodetachment cross section, where we use results from effective range theory (Armstrong 1963; Ohmura & Ohmura 1960) and conservation of energy ($h\nu = \Delta E + \text{K.E.} = \Delta E + \frac{p_e^2}{2m}$, where ΔE is simply the H^- ground state energy, proportional

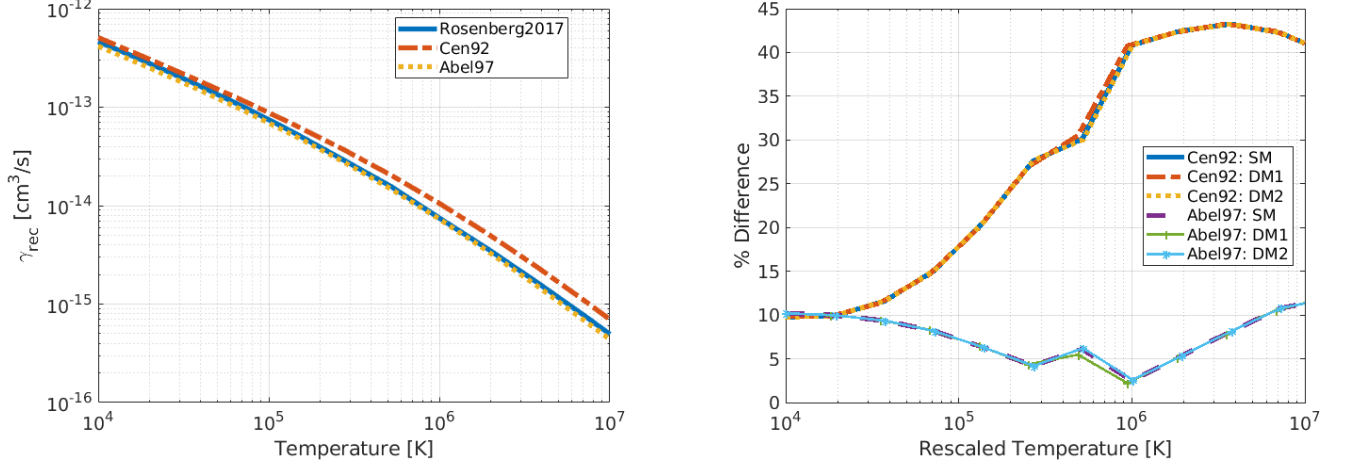


Figure 3. Comparisons between our re-scaled recombination rates from Eq. (4.17) and (4.18) based on Cen (1992) and Abel et al. (1997) and the full rate given in Rosenberg & Fan (2017). On the left we plot the Standard Model rates, equivalent to setting $r_\alpha = r_m = r_M = 1$. On the right we compute the percent difference between the Rosenberg and Cen and Rosenberg and Abel curves, e.g. $\% \text{ Difference}(\text{Ros}, \text{Cen}) = 100\% \frac{|\gamma_{\text{Ros}} - \gamma_{\text{Cen}}|}{\gamma_{\text{Ros}}}$. We have plotted the rates using $m = \{511, 40, 10\} \text{keV}$, $M = \{0.938, 40, 100\} \text{GeV}$, and $\alpha = \{0.00729, 0.01, 0.01\}$, labeled {SM, DM1, DM2}, as a function of the re-scaled temperature, $\tilde{T}_a = r_\alpha^{-2} r_m^{-1} T$. Note that the increased difference between the Rosenberg and Cen curves in both plots arises from Cen being a simplified analytic fit.

to E_{H}) such that

$$\begin{aligned} \sigma_{\text{pd}}(\nu) &= \frac{1}{1 - \gamma \varrho} \frac{16\pi}{3} \frac{\alpha \hbar^2}{\mu} \frac{\Delta E^{1/2} (h\nu - \Delta E)^{3/2}}{(p_e^2/2m + \Delta E)^3} \\ &\propto \frac{1}{1 - \gamma \varrho} \frac{\alpha}{\mu} \frac{y x^3}{T (x^2 + y^2)^3} \end{aligned} \quad (4.19)$$

with $\frac{\gamma^2}{2} = 0.02775 \text{ a.u.}^2$ the electron affinity of hydrogen, and $\varrho = 2.646 \text{ a.u.}$ the effective range (de Jong 1972) in the Standard Model. The effective range ϱ , having dimensions of length, must be proportional to a_0 . The electron affinity is defined in Bethe (1949) as $\frac{\gamma^2}{2} = \frac{\mu \Delta E}{2\hbar} \propto m^2 \alpha^2$, so $\gamma \propto 1/a_0$. Thus, the re-scaling in the two terms effectively cancels, and we can ignore the parametric dependence of the $1/(1 - \gamma \varrho)$ term.

We then find the cross-section for hydrogen electron attachment (reaction 3 on our Table) from the Milne relation [Eq. (4.10)] and $\mu = m$,

$$\sigma_3(x, y) \propto \frac{\alpha}{\mu^2} \frac{x y}{(x^2 + y^2)}, \quad (4.20)$$

which re-scales as [Eq. (4.6)]

$$\gamma_{3, \text{DM}}(T) \approx r_\alpha^2 r_m^{-2} \gamma_{3, \text{SM}}(\tilde{T}_a). \quad (4.21)$$

The full Standard Model rate is given as (Galli & Palla 1998)

$$\gamma_{3, \text{SM}}(T) = 1.4 \times 10^{-18} \text{ erg cm}^{-3} \text{ s}^{-1} T^{0.928} \exp\left(\frac{T}{16200}\right), \quad (4.22)$$

and so the final, re-scaled dark rate is

$$\begin{aligned} \gamma_{3, \text{DM}}(T) &= 1.4 \times 10^{-18} \text{ erg cm}^{-3} \text{ s}^{-1} [r_\alpha^{0.1444} r_m^{-2.928}] \\ &\quad \times T^{0.928} \exp\left(\frac{T}{16200 r_\alpha^2 r_m}\right). \end{aligned} \quad (4.23)$$

Comparing this result with Eq. (4.17), we note that, while both rates use the same overall pre-factor $g(r_\alpha, r_m, r_M)$, the final re-scalings are quite different. This divergence highlights the necessity of including the $r_{\Delta E} = r_\alpha^2 r_m$ temperature re-scaling factor.

Conveniently, Eq. (4.8), (4.19) and $\mu = m$ are sufficient to find the re-scaling for the H^- photodetachment rate, giving

$$\gamma_{4, \text{DM}} \approx r_\alpha^5 r_m \gamma_{4, \text{SM}}(\tilde{T}_a). \quad (4.24)$$

4.4. Reaction 7: mutual neutralization

The cross section for the mutual neutralization reaction, $\text{H}^- + p \rightarrow 2\text{H}$, was computed from the Landau-Zener transition probability at the initial and final potential energy curve pseudo-crossing (Bates & Lewis 1955). Although there are two possible final states, $\text{H}(1s)\text{H}(2s \text{ or } p)$ and $\text{H}(1s)\text{H}(3s, p, \text{ or } d)$, for our purposes the resulting cross section is effectively

$$\sigma_7 \propto R^2 \left(\frac{k_f^2}{k_i^2}\right) F_3(\zeta), \quad (4.25)$$

where $R \propto a_0$ is the internuclear distance at the potential crossing point, k_i and k_f are the momentum of

the initial state and final states, with $k_i^2 \propto \mu \text{K.E.}$ and $k_f^2 \propto k_i^2 + \mu \Delta E = \mu (\text{K.E.} + \Delta E)$, $F_3(\zeta) = \zeta^{n-1} \Gamma(n-1, \zeta) - (2\zeta)^{n-1} \Gamma(n-1, 2\zeta)$ and $\Gamma(n-1, \zeta)$ is the incomplete gamma function. The term ζ is a dimensionless ratio of momenta, which, after some simplification, can be written as $\zeta \propto \frac{1}{k_f} \frac{\alpha \mu \Delta U}{\Delta E^2}$, and ΔU and ΔE are the zeroth order and true potential energy curve differences. In our parameter regime of interest, $\zeta \ll 1$ and a series expansion gives $F_3(\zeta) \approx \zeta$. Then we have

$$\begin{aligned} \sigma_7 &\propto a_0^2 \left(\frac{\text{K.E.} + \Delta E}{\text{K.E.}} \right) \left(\frac{\alpha \sqrt{\mu} \Delta U}{\Delta E^2 \sqrt{\text{K.E.} + \Delta E}} \right) \\ &\propto \alpha a_0^2 \sqrt{\mu} \frac{\sqrt{\text{K.E.} + \Delta E}}{\text{K.E.} \Delta E} \\ &\propto \frac{\alpha a_0^2 \sqrt{\mu}}{T^{3/2}} \frac{\sqrt{x^2 + y^2}}{x^2 y^2} \end{aligned} \quad (4.26)$$

where, in the second line, we used the fact that ΔU and ΔE are proportional. Then, since ΔE is proportional to the atomic binding energy and μ here is the proton mass, we obtain a net re-scaling of

$$\gamma_{7,\text{DM}} \approx r_\alpha^{-3} r_m^{-3} \gamma_{7,\text{SM}}(\tilde{T}_a). \quad (4.27)$$

4.5. Reactions 10 and 15: Langevin and detailed balance

An interaction without a short-range potential barrier will always occur as long as the incoming particle passes the centrifugal potential barrier and spirals into the target. These reactions can be well-treated by classical capture models, the theory of which is presented in e.g. Hirasawa (1969); Zhang & Willitsch (2018). In this approach, the long-range potential which governs the reaction can be written as a series in powers of the separation R :

$$V(R) = - \sum_n \frac{C_n}{R^n}. \quad (4.28)$$

The leading order term in this series dominates in general, and in the Langevin (charge-induced dipole) case, $n = 4$, $C_4 = pe^2/2$ where p is the isotropic polarizability of the molecule, proportional to the trace of p_{ij} . The reaction occurs if the collision energy exceeds the maximum of $V_{\text{eff}}(R) = V(R) + V_{\text{centrifugal}}(R)$, where we include a centrifugal term, $V_{\text{centrifugal}}(R)$, to account for a non-zero impact parameter. Then, since the impact parameter is proportional to the angular momentum, we obtain the cross section in the Langevin case:

$$\sigma_{\text{Lang}}(x) \propto \sqrt{\frac{pe^2}{x^2 k_B T}} \propto \sqrt{\frac{a_0^3 \alpha}{T}} \frac{1}{x}, \quad (4.29)$$

where we have used the property that $p \propto a_0^3$. Then using our tools from Section 4.1 and the definition $\mu \approx M$, we obtain an approximate rate re-scaling of

$$\gamma_{\text{Lang,DM}}(T) \approx r_\alpha^{-1} r_m^{-3/2} r_M^{-1/2} \gamma_{\text{Lang,SM}}(\tilde{T}_a), \quad (4.30)$$

which we will use for both of the Langevin-type reactions: associated detachment of H and H⁻ (H⁻ + H → H₂ + e) and H₂ formation due to H₂⁺ (H₂⁺ + H → H₂ + p).

The computation for the inverse reaction, H₂⁺ charge exchange (H₂ + p → H₂⁺ + H), cross section uses the more general detailed balance results combined with the Langevin cross section. In this case, we have $p_{10} = \mu_{10} v_{10} \approx \mu_{15} v_{15} = p_{15}$ (where the labels 10 and 15 correspond to those reactions), since $\mu_{10} = \frac{m_{\text{H}_2^+} m_{\text{H}}}{m_{\text{H}_2^+} + m_{\text{H}}} \approx \frac{2M^2}{3M} \approx \frac{m_{\text{H}_2} M}{m_{\text{H}_2} + M} \approx \mu_{15}$. With the standard assumption that the internal degrees of freedom g_{10} and g_{15} stay constant, we have $\sigma_{15} \propto \sigma_{10}$, and we only need the temperature re-scaling, which, from reaction 10, is proportional to the hydrogen binding energy E_{H} .

5. VALIDITY OF RESULTS

There are several limitations to the results presented above, some of which are based on assumptions we have made, whereas others follow from the dependence on Standard Model chemistry. Therefore, many of the results so far presented are only valid in certain regions of the parameter space and we discuss the reasons and regions here.

5.1. Limitations inherited from Standard Model results

The largest source of inaccuracy of our results follows from our dependence on the Standard Model rates. Many of the reactions, especially those considered “unimportant” (in Table 3) are poorly known, while others are only known for specific cases. For example, the reaction H⁻ + p → 2H was only known to within an order of magnitude until recently (Glover 2015b), while higher vibrational levels in the H₂ + e → H + H⁻ reaction were not thought to have a significant contribution to the net rate until Capitelli et al. (2007).

Most of the reactions listed in Table 2 are obtained from older cross sections that may not account for these corrections and special cases found more recently. However, we expect that as long as the approximations used in the older rates remain reflective of the underlying physics, the rate re-scalings obtained will remain valid, as demonstrated in Figures 1 and 3.

Additionally, the majority of reaction cross sections listed in section 4 are analytic fits to numerical computations or even experimental data. As such, they are only defined for certain temperature regimes. For example,

the reaction $\text{H} + p \rightarrow \text{H}_2^+ + \gamma$ has a reaction rate defined on the interval $1 \text{ K} \leq T \leq 32000 \text{ K}$, but is undefined elsewhere. Extrapolation past those temperature limits can result in significant divergences, especially with some of the more accurate fits that have strong exponential terms, like the rovibrational cooling rates mentioned in Section 3. These temperature limits will scale with the dark parameters but extra care should still be taken when exploring more extreme parameter space ranges.

A more subtle issue exists for radiative reactions because the gas and photons need not share a temperature. In principle, the reaction rates should then depend on both the gas and photon temperature, but all of our rates depend on only one of these temperatures. Cyr-Racine & Sigurdson (2013) points out that in particular the standard calculation of the recombination coefficient neglects stimulated recombination, which explicitly depends on the photon temperature. That work found a change of at most a factor of a few in the recombination coefficient due to this effect when $T_g = 0.01T_\gamma$. In the particular case of hydrogen recombination, this issue is relevant only for weakly coupled dark matter models, since otherwise the gas and radiation are thermally coupled at recombination. For the problem of halo formation (Grassi et al. 2014), the matter and radiation do not in general share a temperature, but even so standard calculations consider each rate to be a function of only one temperature.

A final limitation derives from several of the rates listed here depending on the assumption from the Standard Model that $m \ll M$. Trivially, in many cases we approximate the reduced mass $\mu = \frac{mM}{m+M} \approx m$, or $\mu \approx m_H \approx M$, which can be easily adjusted as $m \rightarrow M$. On the other hand, in section 2 we assumed stationary nuclei, with electronic motion resulting in minor corrections at most. This no longer holds as $m \rightarrow M$, affecting both the fundamental wave functions, as we can no longer use the Born-Oppenheimer approximation, and cross section calculations. For example, the derivation for the hydrogen electron attachment reaction ($\text{H} + e \rightarrow \text{H}^- + \gamma$) assumed a massive stationary, screened proton captures a free electron. In the extreme case, $m \approx M$, the physics should become much closer to positronium production, $e^- + e^+ \rightarrow Ps$ or radiative association of H and p, $\text{H} + p \rightarrow \text{H}_2^+ + \gamma$, with the corresponding re-scaling, but where and how the transition would occur is beyond the scope of this work. Even the basic hydrogen atomic physics are modified; with a significantly larger electron mass, the energy eigenvalues would have a significant dependence on the nuclear (proton) mass (Poszwa et al. 2016).

5.2. Comparison with deuterated chemistry

As mentioned in the introduction, we can compare our rates with those obtained for deuterium reactions. Gay et al. (2011) has compiled a significant list of deuterium reaction rates; while the majority are computed using the mass re-scaling described in Appendix A, or assumed identical to the hydrogen rate (e.g. $\text{D}^+ + e \rightleftharpoons \text{D} + \gamma$), one is based directly on experimental data. The reaction $\text{D}_2 + \text{D}^+ \rightarrow \text{D}_2^+ + \text{D}$ has a rate derived from the cross section listed in Wang & Stancil (2002) and given by

$$\begin{aligned} & \gamma_{\text{D}_2+\text{D}^+\rightarrow\text{D}_2^++\text{D}} \\ &= 2.46 \times 10^{-9} \text{ cm}^3 \text{ s}^{-1} T_3^{-0.439} \exp\left(\frac{-30500}{T}\right). \end{aligned} \quad (5.1)$$

While this appears significantly different to our re-scaled result from Galli & Palla (1998), $\gamma_{15,\text{DM}} \approx 2.12 \times 10^{-10} \text{ cm}^3 \text{ s}^{-1} \exp\left(\frac{-21050}{T}\right)$, the discrepancy is not fatal to our argument. Savin et al. (2004) points out that there is significant variation between the reported rates for the $\text{H}_2 + \text{H}^+ \rightarrow \text{H}_2^+ + \text{H}$ reaction, with sometimes drastically different values and temperature behavior even between rates based on the same source data. While the rates may differ significantly, they share common features, including an exponential drop off dependent on the threshold energy at low temperatures, and minimal temperature dependence in the 10^4 K to $10^{4.5} \text{ K}$ range. In Figure 4, we plot several re-scaled hydrogen rates (from Galli & Palla (1998); Abel et al. (1997); Savin et al. (2004)), as well as the rate from Gay, to demonstrate that the rates are sufficiently similar, especially at higher temperatures.

As stated, the remaining pure deuterium reactions in Gay et al. not identical to hydrogen rates have been computed using the mass re-scaling method described in section A, with a minor change: in Eq. (A2), $a_{2,\text{known}} \rightarrow a_{2,\text{known}} + 0.5$. To the extent that those rates have been used in many astrochemistry calculations, this further validates our approach of re-scaling known Standard Model rates, and comparison of Eq. (A3) with Eq. (4.2) and Eq. (4.6) reveals that the simplified version is equivalent to $g(r_\alpha, r_m, r_M) = r_\mu^{-1/2-a/2}$ and ΔE at least approximately independent of μ . Since $\mu \propto M$ for these cases, this holds reasonably well for those reactions with simple cross sections and atomic binding energy, e.g. mutual neutralization, $\text{H}^- + p \rightarrow 2\text{H}$. Our more complete re-scaling procedure ($\gamma_{7,\text{DM}} \propto r_M^{-0.5} \gamma_{7,\text{SM}}$) gives equivalent results to the mass re-scaling ($\gamma_{7,\text{DM}} \propto r_M^{-0.487} \gamma_{7,\text{SM}}$).

Lastly, we consider the cooling rates and demonstrate why we do not validate using HD chemistry. Unfortunately, we were unable to find a D_2 cooling function

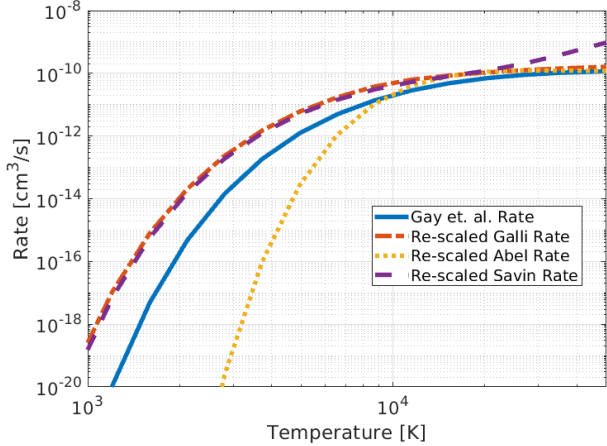


Figure 4. $D_2 + D^+ \rightarrow D_2^+ + D$ reaction rate and re-scaled H rates for comparison. Re-scaled $H_2 + H^+ \rightarrow H_2^+ + H$ reaction rates are from Galli & Palla (1998); Abel et al. (1997); Savin et al. (2004) and the deuterium rate is from Gay et al. (2011). The deuterium rate is clearly comparable to the re-scaled hydrogen rates to the extent that they are comparable to each other.

based on experimental data or theoretical calculations and can only compare our re-scaled rates to HD cooling rates, setting $M = 1.5m_p$. However, HD has significantly different behavior, as compared to H_2 , due to its mass asymmetry-induced dipole moment and allowance of $J \pm 1$ transitions. Thus, the cooling comparison breaks down in the low temperature regime where those aspects become relevant. We demonstrate this issue in Figure 5, where we plot the re-scaled Hollenbach and Glover H_2 cooling rates versus the HD cooling rate from Glover & Abel (2008). Note that while the differences between the HD curve and the re-scaled curves are small in the high temperature region, at low temperatures the HD curve is orders of magnitude higher.

5.3. Additional reactions

Galli & Palla (1998) include several reaction rates not considered in the above sections, briefly listed in Table 3. We have skipped these reactions for several reasons, including being three-body reactions, such as $H_2 + e \rightarrow 2H + e$, or having “irrelevant” rates, like $H_2^+ + H \rightarrow H_3^+ + \gamma$. Most importantly, these reactions were not considered to be part of the minimal model required to compute the evolution of H, H^+ , H_2 , and H_2^+ . As such, we determined that it was more valuable to provide a minimal list of reactions and the tools to re-scale others as needed, than to attempt to re-scale all of them. Note that this does not mean the reactions included in Table 2 are sufficient in all cases. As an example, reaction 18, $H_2 + \gamma \rightarrow H_2^+ + e$, is not considered part of Galli & Palla (1998)’s minimal model, but we

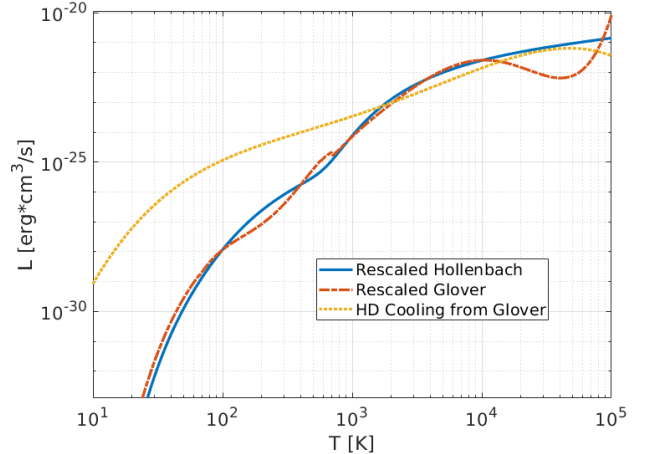


Figure 5. Demonstration of the inability to utilize the HD molecule in validation. While the re-scaled Hollenbach and Glover cooling curves are similar to the HD cooling curve in the high temperature region, at low temperatures the allowed $J \pm 1$ transitions enable HD to have an orders of magnitude higher cooling rate.

Reaction	Reaction
6 $H + p \rightarrow H_2^+ + e$	17 $H_2 + e \rightarrow 2H + e$
11 $H_2^+ + e \rightarrow 2H$	19 $H_3^+ + H \rightarrow H_2^+ + H_2$
12 $H_2^+ + \gamma \rightarrow 2p + e$	20 $H_3^+ + e \rightarrow H_2 + H_D$
13 $H_2^+ + H_2 \rightarrow H_3^+ + H_D$	21 $H_2 + H^+ \rightarrow H_3^+ + \gamma$
14 $H_2^+ + H \rightarrow H_3^+ + \gamma$	22 $H_3^+ + \gamma \rightarrow H_2^+ + H_D$
16 $H_2 + e \rightarrow H + H^-$	

Table 3. Reactions from Galli and Palla that were not included in the re-scaling procedure. These reactions are not part of the minimal model considered by Galli and Palla.

computed the necessary re-scaling because it warranted inclusion in certain regions of the dark parameter space in our companion work (Gurian & Jeong 2021).

6. CONCLUSION

In order to complete the study of “atomic” dark matter models and determine their impact on the formation and evolution of large-scale structure, galactic halos, and compact object, we have extended previous studies (Rosenberg & Fan 2017; Buckley & DiFranzo 2018; Boddy et al. 2016) by calculating the chemistry of dark molecular hydrogen. As dark molecular hydrogen processes dominate the chemistry at low temperature, this work provides an essential tool for studying the formation and evolution of low-mass halos with much lower virial temperatures, and the end point of cooling processes within halos.

We have provided some basic tools for working with dark molecules, including the re-scaling for several key atomic and molecular quantities (Table 1), and the pro-

cedure for obtaining approximately re-scaled rates when the physics of the analogous Standard Model interaction is known (e.g. Eqs. (2.25, 4.2, & 4.6)). We applied these tools to two important areas in molecular chemistry: thermal processes and chemical reactions, and determine how the rates in a minimal subset of these processes can be re-scaled to obtain expressions valid for a wide range of dark matter parameters (Eqs. (3.23, 3.34, & 3.36) and Table 2). Importantly, these re-scaled rates are only as accurate as the original Standard Model rates and neither correct nor transcend any limitations or assumptions therein, as demonstrated with our comparison with deuterated reactions (Eq. 5.1 and Figures 4 & 5).

Additionally, we note that many astrochemical databases and chemical models either neglect deuterium reactions entirely, or when present either use the hydrogen rate directly or use the simplified mass re-scaling method from Appendix A (e.g. the `deuspin` chemical network in the KIDA database, from Majumdar et al. (2016)). Therefore, at a minimum we expect the re-scaling method presented here to provide improved rates for deuterium reactions that can easily be included in said models.

We have provided the first calculations of dark molecular processes with sufficient accuracy to be used in simulations. These are used in our companion papers to derive cosmic abundances of various states (ionized, atomic, and molecular hydrogen) (Gurian & Jeong 2021) and to model the low-virial temperature halo formation in analogous fashion to the minihalo formation in Standard Model (Ryan & Shandera 2021). Eventually, these rates and the re-scaling procedure can be used to validate phenomenological models used in large-scale structure simulations for studying the formation and evolution of dark-matter halos, which increasingly depend on full numerical calculations that depend on chemistry rates that we study here.

At the core of the atomic dark-matter halo, the dark-matter density may reach high enough value so that the re-scaling of other process rates, especially many-body processes such as H_3 reactions, might also be necessary. Of course, to get the dark-chemistry rates, one can also take the parallel approach of computing the interaction rates from the first-principle quantum calculations. We leave these computations for future work.

ACKNOWLEDGMENTS

Funding for this work was provided by the Charles E. Kaufman Foundation of the Pittsburgh Foundation.

APPENDIX

A. BRIEF REVIEW OF MASS RE-SCALING

Applications of chemistry in astrophysics frequently require chemical reaction rates that are difficult to compute from first-principles, and are required in temperature and density regimes inaccessible in laboratory experiments on Earth. Sometimes, rates may be known for other isotopes or related species and in these cases a common approach in the literature (see e.g. Stancil et al. (1998); Walker et al. (2014)) is similar to what we present in this work: re-scaling the known rate by a ratio of the masses.

Assuming the known (endoergic) reaction rate can be approximated by the form

$$\gamma_{\text{known}} = a_1 T^{a_2} \exp\left(\frac{a_3}{T}\right), \quad (\text{A1})$$

with temperature T and constants a_i , then in the mass-scaled rate the coefficient a_1 takes the form

$$a_{1,\text{new}} = a_{1,\text{known}} \left(\frac{\mu_{\text{known}}}{\mu_{\text{new}}}\right)^{a_{2,\text{known}}}, \quad (\text{A2})$$

where μ_{known} (μ_{new}) is the reduced mass of the known (new) reaction. All other terms remain the same and the same formula holds for exoergic rates. For example, the rate coefficient for deuterium mutual neutralization, $D^- + D^+ \rightarrow 2D$ can be approximately obtained by re-scaling the rate for the regular hydrogen reaction, $H^- + p \rightarrow 2H$. The hydrogen reaction is known to be of the form of Eq.(A1) with $a_1 = 1.4 \times 10^{-7} \text{ cm}^3 \text{ s}^{-1}$ and $a_2 = -0.487$ (Stancil et al. 1998). Using $\mu_D \approx 1 \text{ GeV}$ and $\mu_H \approx 0.5 \text{ GeV}$, the mass re-scaling procedure suggests the corresponding deuterium process is proportional to $a_{1,D} = a_{1,H} \left(\frac{\mu_H}{\mu_D}\right)^{a_{2,H}} \approx 1.4 a_{1,H} = 1.96 \text{ cm}^3 \text{ s}^{-1}$.

The derivation of this re-scaling relationship is straightforward (Walker et al. 2014). Assume the reaction cross section depends on the collision velocity v as

$$\sigma(v) = Bv^a, \quad (\text{A3})$$

where B is a mass independent constant with units $[\text{length}]^{2-a}[\text{time}]^a$. The rate is given by the thermal average,

$$\gamma = \langle \sigma v \rangle = \left(\frac{2}{\pi}\right)^{1/2} \left(\frac{\mu}{k_B T}\right)^{3/2} \int_0^\infty \sigma(v) \exp(-\mu v^2/2k_B T) v^3 dv. \quad (\text{A4})$$

The integral can be performed exactly, giving

$$\gamma = \frac{B}{\sqrt{\pi}} 2^{\frac{a+3}{2}} \left(\frac{k_B T}{\mu}\right)^{\frac{a+1}{2}} \Gamma\left(\frac{a}{2} + 2\right) = A(a) \left(\frac{T}{\mu}\right)^b. \quad (\text{A5})$$

Then re-scaling μ gives back the expression found in Eq. (A2), where $a_1 = A(a)\mu^{-b}$ and $a_2 = b = \frac{1}{2}(a+1)$. Note that the exponential cutoff in Eq. (A1) not derived in Walker et al. (2014) can arise naturally within this formalism in at least two ways. First, by imposing a lower energy cutoff in the integration:

$$\gamma = \left(\frac{2}{\pi}\right)^{1/2} \left(\frac{\mu}{k_B T}\right)^{3/2} \int_{v_{min}}^\infty \sigma(v) \exp(-\mu v^2/2k_B T) v^3 dv \quad (\text{A6})$$

$$= \frac{B}{\sqrt{\pi}} 2^{\frac{a+3}{2}} \left(\frac{k_B T}{\mu}\right)^{\frac{1+a}{2}} \Gamma\left(2 + \frac{a}{2}, \frac{\mu v_{min}^2}{2k_B T}\right), \quad (\text{A7})$$

and approximating the incomplete gamma function in $1/T$ by an exponent in $-1/T$ (which is exact for $a = -2$). Second, if there is no minimum energy cutoff in the forward reaction (i.e. Langevin reactions), an exponential term will appear in the reverse reaction due to the detailed balance factor. This can give us some confidence that the form Eq. (A2) is physically well motivated and could be reasonable to re-scale empirical fits of this form over a wide temperature range.

Unfortunately, Eq. (A2) is insufficient for computing dark reaction rates for two reasons. First, it clearly cannot capture the effect of allowing α and m to vary from their standard model values. Second, even in the case where $r_\alpha = r_m = 1$, the B term in Eq. (A3) is dimensionful, and often contains factors of μ that are not accounted for. Likewise, the dimensionful a_2 and a_3 terms in Eq. (A1) can depend on m , M , and α , significantly changing the rate's temperature dependence. The re-scaling procedure we have presented in this paper overcomes these limitations.

B. QUADRUPOLEAR SPONTANEOUS EMISSION IN ATOMIC UNITS

The quadrupolar spontaneous emission rate is usually given in atomic units in the literature. In these units, $e^2 = 4\pi\epsilon_0 = \hbar \equiv 1$, masses are measured in $m_e \equiv 1$, and energy is measured in units of the Hartree energy, $E_H = \alpha^2 m_e c^2 = 1$. With these definitions, $c = 1/\alpha$, and the unit of time is \hbar/E_H .

When the energies and quadrupole moments are given in atomic units, the rate for a standard model hydrogen atom to transition from a state with (vibrational, rotational) quantum numbers $(\nu', J+2)$ to the state with (ν, J) is (Turner et al. 1977; Flower 2007)

$$\begin{aligned} A(\nu, J \leftarrow \nu', J+2) &= (1.43 \text{ } 10^4 \text{ s}^{-1}) (E_{\nu', J+2} - E_{\nu, J})^5 \frac{3(J+2)(J+1)}{2(2J+5)(2J+3)} Q_{\nu', J+2; \nu, J}^2 \\ &= \frac{1}{60c^5} (E_{\nu', J+2} - E_{\nu, J})^5 \frac{3(J+2)(J+1)}{2(2J+5)(2J+3)} Q_{\nu', J+2; \nu, J}^2 \end{aligned} \quad (\text{B1})$$

The rates for other transitions, with $\Delta J = 0, -2$, have the same form. The numerical pre-factor in the top line can be obtained from the second line using the conversion to S.I. units from the unit of time in atomic units, \hbar/E_H , ($\hbar/E_H = 2.418884 \times 10^{-17}$ s in S.I. units), $c = 137$, and the factor of 60 (note the typo in Flower (2007)).

From Eq.(B1), the re-scaling relationships needed to approximate dark matter transition rates can be determined as a change in units from Standard Model atomic units to dark matter atomic units. Given a numerical value of some transition rate in the Standard Model, the parametric dependence comes from changing units in the factor of $E_H/c^5 = E_H \alpha^5$ in the pre-factor in Eq. (B1), and from the fundamental constants appearing in the energy difference

of vibrational or rotational modes when those energies are expressed in atomic units. Since the quadrupole moment is proportional to a_0^2 , there is no additional parametric dependence from Q^2 . That is, suppose a Standard Model quadrupole in S.I. units is $Q \equiv \tilde{Q}a_0^2$, where \tilde{Q} is value of the quadrupole in Standard Model atomic units. Then the dark matter quadrupole can be obtained by $Q^{\text{DM}} = Q \left(\frac{a_{0,\text{DM}}}{a_0}\right)^2$. Using dark atomic units on the left hand side, $\tilde{Q}^{\text{DM}} = Q \left(\frac{1}{a_0}\right)^2$, or $\tilde{Q}^{\text{DM}} = \tilde{Q}$.

Finally, then, the dark matter Einstein A coefficient for transitions between rotational levels can be estimated by the re-scaling

$$\begin{aligned} A_{\text{quad,rot DM}} &= \left[\left(\frac{\alpha_{\text{DM}}}{\alpha_{\text{SM}}} \right)^5 \frac{E_{\text{h, DM}}}{E_{\text{h SM}}} \right] \left[\left(\frac{\Delta E_{\text{rot,DM}}}{\alpha_{\text{DM}}^2 m_e c^2} \right) \left(\frac{\alpha_{\text{SM}}^2 m_e c^2}{\Delta E_{\text{rot,SM}}} \right) \right]^5 A_{\text{quad,rot SM}} \\ &= \left[\frac{r_\alpha^7 r_m^6}{r_M^5} \right] A_{\text{quad,rot, SM}} \end{aligned} \quad (\text{B2})$$

and, for vibrational transitions,

$$\begin{aligned} A_{\text{quad,vib DM}} &= \left[\left(\frac{\alpha_{\text{DM}}}{\alpha_{\text{SM}}} \right)^5 \frac{E_{\text{h, DM}}}{E_{\text{h SM}}} \right] \left[\frac{\Delta E_{\text{vib,DM}}}{\alpha_{\text{DM}}^2 m_e c^2} \frac{\alpha_{\text{SM}}^2 m_e c^2}{\Delta E_{\text{vib,SM}}} \right]^5 A_{\text{quad,vib SM}} \\ &= \left[\frac{r_\alpha^7 r_m^{7/2}}{r_M^{5/2}} \right] A_{\text{quad,vib SM}}. \end{aligned} \quad (\text{B3})$$

These expressions agree with those obtained in the main text.

C. RE-SCALING COMBINED COOLING RATE

The literature on molecular hydrogen cooling rates tends to present the low-density limit as a single analytic fit of the full experimental or numerical rovibrational results, $\mathcal{C}_{\text{rovib}}$ (see e.g. Galli & Palla (1998); Glover & Abel (2008)). This presents a difficulty in applying the re-scaling procedure presented here because the cooling process is composed of different physical processes, apparently complicating our assumption of a single energy scale by which the process can be non-dimensionalized and the fit re-scaled (a problem not unique to molecular cooling). Here, we show how these complications can be resolved by applying piecewise re-scalings in the temperature regime relevant to each physical process.

The rescaling of the temperature regimes themselves may lead to a gap between the rescaled curves. In this case, the higher temperature process is strongly suppressed below threshold and dominates above threshold, so we extrapolate each re-scaling out to the re-scaled threshold temperature and allow these curves to meet with a discontinuous derivative.

For the case of $n \rightarrow 0$ molecular cooling, there are only two processes to consider: rotational and vibrational level transitions. The net rate is the simple sum, $\mathcal{C}_{\text{tot}} = \mathcal{C}_{\text{rot}} + \mathcal{C}_{\text{vib}}$. Further, rotational transitions dominate at low temperatures (insufficient energy to induce a vibrational transition) and vibrational transitions dominate at high temperatures (larger energy transition), with a clear changeover between the regimes. Defining the pivot temperature T_0 as the temperature where the rotational cooling rate equals the vibrational cooling rate, we can divide the total rovibrational rate into

$$\mathcal{C}_{\text{rovib}}(T) = \mathcal{C}_{\text{rovib}, T < T_0}(T) + \mathcal{C}_{\text{rovib}, T \geq T_0}(T) = R(T) + V(T). \quad (\text{C1})$$

Note that $R(T)$ is only defined on the interval $0 < T \leq T_0$ and $V(T)$ is only defined on the interval $T_0 \leq T < \infty$.

The results from Eq. (3.21) and (3.32) give the re-scalings for R and V ,

$$R_{\text{DM}}(T) = r_\alpha r_m r_M^{-2} R_{\text{SM}}(\tilde{T}_r) \quad (\text{C2})$$

$$V_{\text{DM}}(T) = r_\alpha r_m^{1/4} r_M^{-5/4} V_{\text{SM}}(\tilde{T}_v). \quad (\text{C3})$$

But, since R and V are only defined for $T \leq T_0$ and $T \geq T_0$, R_{DM} is only defined for $T \leq \frac{r_\alpha^2 r_m^2}{r_M} T_0 = T_{0,r}$ and V_{DM} is only defined for $T \geq \frac{r_\alpha^2 r_m^{3/2}}{r_M^{1/2}} T_0 = T_{0,v}$. Thus, the sum of R_{DM} and V_{DM} only gives the re-scaled rovibrational cooling

rate across all T if $T_{0,r} \geq T_{0,v}$ (effectively $\frac{r_M}{r_m} \leq 1$), i.e.

$$C_{\text{rovib,DM}}(T) = R_{\text{DM}}(T) + V_{\text{DM}}(T) \iff r_M \leq r_m. \quad (\text{C4})$$

The other case, $r_M > r_m$, requires additional information to fill the two gaps, $T_{0,r} < T \leq T_{0,\text{DM}}$ and $T_{0,\text{DM}} \leq T < T_{0,v}$, where $T_{0,\text{DM}}$ is the re-scaled pivot point. One option exploits the high (low) temperature behavior of the rotational (vibrational) analytic curves from [Hollenbach & McKee \(1979\)](#). Essentially, the rotational and vibrational curves both behave logarithmically at the temperature extremes, so a linear extrapolation of R_{DM} from $T_{0,r}$ to $T_{0,\text{DM}}$ and of V_{DM} from $T_{0,v}$ to $T_{0,\text{DM}}$ provides an acceptable fit.⁵ The final full rovibrational cooling curve is given by

$$C_{\text{rovib,DM}}(T) = \begin{cases} R_{\text{DM}}(T) + V_{\text{DM}}(T) & r_M \leq r_m \\ R_{\text{DM}}(T) & r_M > r_m \text{ \& } T \leq T_{0,r} \\ \text{linExtrap}(R_{\text{DM}}(T)) & r_M > r_m \text{ \& } T_{0,r} < T < T_{0,\text{DM}} \\ \text{linExtrap}(V_{\text{DM}}(T)) & r_M > r_m \text{ \& } T_{0,\text{DM}} \leq T < T_{0,v} \\ V_{\text{DM}}(T) & r_M > r_m \text{ \& } T_{0,v} \leq T \end{cases}, \quad (\text{C5})$$

where $\text{linExtrap}(F(T))$ is the linear extrapolation of the function $F(T)$. This is the approach taken in [Figures 1 and 2](#). Other possibilities include different extrapolation functions or simply using the [Hollenbach and McKee](#) rates in those regions.

Using the rotational and vibrational rates from [Hollenbach & McKee \(1979\)](#), we find for $H_2 - H$ collisions that $T_0 = 856 \text{ K}$ and $T_{0,\text{DM}} \approx \left[r_\alpha^2 r_m^{3/2} r_M^{-0.54} \right] T_{0,\text{SM}}$ across the parameter space used in [Figures 1 and 2](#). For $H_2 - H_2$ collisions, we find $T_0 = 5.40 \times 10^3 \text{ K}$ and $T_{0,\text{DM}} \approx \left[r_\alpha^2 r_m^{1.58} r_M^{-0.586} \right] T_{0,\text{SM}}$.

REFERENCES

- Aannestad, P. A. 1973, *ApJS*, 25, 223, doi: [10.1086/190268](#)
- Abbott, B. P., et al. 2018, *PhRvL*, 121, 231103, doi: [10.1103/PhysRevLett.121.231103](#)
- . 2019, *PhRvL*, 123, 161102, doi: [10.1103/PhysRevLett.123.161102](#)
- Abel, T., Anninos, P., Zhang, Y., & Norman, M. L. 1997, *NewA*, 2, 181, doi: [10.1016/s1384-1076\(97\)00010-9](#)
- Ackerman, L., Buckley, M. R., Carroll, S. M., & Kamionkowski, M. 2009, *PhRvD*, 79, 023519, doi: [10.1103/PhysRevD.79.023519](#)
- Agrawal, P., Cyr-Racine, F.-Y., Randall, L., & Scholtz, J. 2017, *JCAP*, 05, 022, doi: [10.1088/1475-7516/2017/05/022](#)
- Armstrong, B. H. 1963, *Physical Review*, 131, 1132, doi: [10.1103/physrev.131.1132](#)
- Bates, D. R., & Lewis, J. T. 1955, *Proceedings of the Physical Society. Section A*, 68, 173, doi: [10.1088/0370-1298/68/3/306](#)
- Berezhiani, Z., Comelli, D., & Villante, F. L. 2001, *Physics Letters B*, 503, 362, doi: [10.1016/S0370-2693\(01\)00217-9](#)
- Bethe, H., & Jackiw, R. 1997, *Intermediate Quantum Mechanics (Perseus)*
- Bethe, H. A. 1949, *Physical Review*, 76, 38, doi: [10.1103/physrev.76.38](#)
- Boddy, K. K., Kaplinghat, M., Kwa, A., & Peter, A. H. 2016, *PhRvD*, 94, 123017
- Bramante, J., & Elahi, F. 2015, *PhRvD*, 91, 115001, doi: [10.1103/PhysRevD.91.115001](#)
- Bramante, J., & Linden, T. 2014, *PhRvL*, 113, 191301, doi: [10.1103/PhysRevLett.113.191301](#)
- Browne, J. C., & Dalgarno, A. 1969, *Journal of Physics B: Atomic and Molecular Physics*, 2, 885, doi: [10.1088/0022-3700/2/8/309](#)
- Buckley, M. R., & DiFranzo, A. 2018, *PhRvL*, 120, doi: [10.1103/physrevlett.120.051102](#)
- Bullock, J. S., & Boylan-Kolchin, M. 2017, *ARA&A*, 55, 343, doi: [10.1146/annurev-astro-091916-055313](#)
- Capitelli, M., Coppola, C. M., Diomede, P., & Longo, S. 2007, *A&A*, 470, 811, doi: [10.1051/0004-6361:20077600](#)
- Cen, R. 1992, *ApJS*, 78, 341, doi: [10.1086/191630](#)
- Chang, J. H., Egana-Ugrinovic, D., Essig, R., & Kouvaris, C. 2019, *JCAP*, 2019, 036, doi: [10.1088/1475-7516/2019/03/036](#)

⁵ We define linear extrapolation here as fitting the curve of interest, defined on some interval, to a function of the form $y = ax + b$ and evaluating the function outside the interval boundary.

- Choquette, J., Cline, J. M., & Cornell, J. M. 2019, *JCAP*, 2019, 036, doi: [10.1088/1475-7516/2019/07/036](https://doi.org/10.1088/1475-7516/2019/07/036)
- Cyr-Racine, F.-Y., de Putter, R., Raccanelli, A., & Sigurdson, K. 2014, *Phys. Rev. D*, 89, 063517, doi: [10.1103/PhysRevD.89.063517](https://doi.org/10.1103/PhysRevD.89.063517)
- Cyr-Racine, F.-Y., & Sigurdson, K. 2013, *PhRvD*, 87, doi: [10.1103/physrevd.87.103515](https://doi.org/10.1103/physrevd.87.103515)
- D'Amico, G., Panci, P., Lupi, A., Bovino, S., & Silk, J. 2017, *MNRAS*, doi: [10.1093/mnras/stx2419](https://doi.org/10.1093/mnras/stx2419)
- de Jong, T. 1972, *A&A*, 20, 263. <https://ui.adsabs.harvard.edu/abs/1972A&A....20..263D>
- de Lavallaz, A., & Fairbairn, M. 2010, *PhRvD*, 81, 123521, doi: [10.1103/PhysRevD.81.123521](https://doi.org/10.1103/PhysRevD.81.123521)
- Dessert, C., Kilic, C., Trendafilova, C., & Tsai, Y. 2019, *PhRvD*, 100, doi: [10.1103/physrevd.100.015029](https://doi.org/10.1103/physrevd.100.015029)
- Dong, S.-H. 2007, *Factorization Method in Quantum Mechanics* (Springer)
- Draine, B. T. 2011, *Physics of the interstellar and intergalactic medium* (Princeton University Press)
- Dushman, S. 1936, *Journal of Chemical Education*, 13, 287, doi: [10.1021/ed013p287](https://doi.org/10.1021/ed013p287)
- Fan, J., Katz, A., Randall, L., & Reece, M. 2013, *Physics of the Dark Universe*, 2, 139, doi: [10.1016/j.dark.2013.07.001](https://doi.org/10.1016/j.dark.2013.07.001)
- Feng, J. L., Kaplinghat, M., Tu, H., & Yu, H.-B. 2009, *JCAP*, 2009, 004, doi: [10.1088/1475-7516/2009/07/004](https://doi.org/10.1088/1475-7516/2009/07/004)
- Flower, D. 2007, *Molecular collisions in the interstellar medium* (Cambridge University Press)
- Foot, R., & Vagnozzi, S. 2015, *PhRvD*, 91, 023512, doi: [10.1103/physrevd.91.023512](https://doi.org/10.1103/physrevd.91.023512)
- Galli, D., & Palla, F. 1998, *A&A*, 335, 403. <https://arxiv.org/abs/astro-ph/9803315>
- Galli, D., & Palla, F. 2013, *ARA&A*, 51, 163, doi: [10.1146/annurev-astro-082812-141029](https://doi.org/10.1146/annurev-astro-082812-141029)
- Gay, C. D., Stancil, P. C., Lepp, S., & Dalgarno, A. 2011, *ApJ*, 737, 44, doi: [10.1088/0004-637x/737/1/44](https://doi.org/10.1088/0004-637x/737/1/44)
- Ghalsasi, A., & McQuinn, M. 2018, *Phys. Rev. D*, 97, 123018, doi: [10.1103/PhysRevD.97.123018](https://doi.org/10.1103/PhysRevD.97.123018)
- Glover, S. 2005, *SSRv*, 117, 445, doi: [10.1007/s11214-005-5821-y](https://doi.org/10.1007/s11214-005-5821-y)
- . 2012, in *The First Galaxies* (Springer Berlin Heidelberg), 103–174, doi: [10.1007/978-3-642-32362-1_3](https://doi.org/10.1007/978-3-642-32362-1_3)
- Glover, S. C. O. 2015a, *MNRAS*, 453, 2902, doi: [10.1093/mnras/stv1781](https://doi.org/10.1093/mnras/stv1781)
- . 2015b, *MNRAS*, 451, 2082, doi: [10.1093/mnras/stv1059](https://doi.org/10.1093/mnras/stv1059)
- Glover, S. C. O., & Abel, T. 2008, *MNRAS*, 388, 1627, doi: [10.1111/j.1365-2966.2008.13224.x](https://doi.org/10.1111/j.1365-2966.2008.13224.x)
- Grassi, T., Bovino, S., Schleicher, D. R. G., et al. 2014, *MNRAS*, 439, 2386, doi: [10.1093/mnras/stu114](https://doi.org/10.1093/mnras/stu114)
- Gurian, J., & Jeong, D. 2021, In preparation
- Hart, L., & Chluba, J. 2017, *Monthly Notices of the Royal Astronomical Society*, 474, 1850–1861, doi: [10.1093/mnras/stx2783](https://doi.org/10.1093/mnras/stx2783)
- Heitler, W., & London, F. 1927, *Zeitschrift für Physik*, 44, 455, doi: [10.1007/bf01397394](https://doi.org/10.1007/bf01397394)
- Herzberg, G., & Monfils, A. 1961, *Journal of Molecular Spectroscopy*, 5, 482, doi: [10.1016/0022-2852\(61\)90111-4](https://doi.org/10.1016/0022-2852(61)90111-4)
- Hippert, M., Setford, J., Tan, H., et al. 2021, arXiv e-prints, arXiv:2103.01965. <https://arxiv.org/abs/2103.01965>
- Hirasawa, T. 1969, *Progress of Theoretical Physics*, 42, 523, doi: [10.1143/ptp.42.523](https://doi.org/10.1143/ptp.42.523)
- Hollenbach, D., & McKee, C. F. 1979, *ApJ*, 41, 555, doi: [10.1086/190631](https://doi.org/10.1086/190631)
- Hollenbach, D., & McKee, C. F. 1989, *ApJ*, 342, 306, doi: [10.1086/167595](https://doi.org/10.1086/167595)
- Jackson, J. D. 1998, *Classical Electrodynamics*, 3rd Edition (Wiley)
- James, H. M., & Coolidge, A. S. 1933, *JChPh*, 1, 825, doi: [10.1063/1.1749252](https://doi.org/10.1063/1.1749252)
- Kaplan, D. E., Krnjaic, G. Z., Rehermann, K. R., & Wells, C. M. 2010, *JCAP*, 2010, 021, doi: [10.1088/1475-7516/2010/05/021](https://doi.org/10.1088/1475-7516/2010/05/021)
- . 2011, *JCAP*, 2011, 011, doi: [10.1088/1475-7516/2011/10/011](https://doi.org/10.1088/1475-7516/2011/10/011)
- Kołos, W., & Roothaan, C. C. 1960, *Reviews of Modern Physics*, 32, 219, doi: [10.1103/RevModPhys.32.219](https://doi.org/10.1103/RevModPhys.32.219)
- Kołos, W., & Wolniewicz, L. 1965, *JChPh*, 43, 2429, doi: [10.1063/1.1697142](https://doi.org/10.1063/1.1697142)
- . 1967, *JChPh*, 46, 1426, doi: [10.1063/1.1840870](https://doi.org/10.1063/1.1840870)
- Kouvaris, C., & Tinyakov, P. 2011, *PhRvD*, 83, 083512, doi: [10.1103/PhysRevD.83.083512](https://doi.org/10.1103/PhysRevD.83.083512)
- Kouvaris, C., Tinyakov, P., & Tytgat, M. H. G. 2018, *PhRvL*, 121, 221102, doi: [10.1103/PhysRevLett.121.221102](https://doi.org/10.1103/PhysRevLett.121.221102)
- Latif, M., Lupi, A., Schleicher, D., et al. 2019, *Mon. Not. Roy. Astron. Soc.*, 485, 3352, doi: [10.1093/mnras/stz608](https://doi.org/10.1093/mnras/stz608)
- Li, H., Wu, J., Zhou, B.-L., Zhu, J.-M., & Yan, Z.-C. 2007, *PhRvA*, 75, 012504, doi: [10.1103/physreva.75.012504](https://doi.org/10.1103/physreva.75.012504)
- Low, C., & Lynden-Bell, D. 1976, *MNRAS*, 176, 367, doi: [10.1093/mnras/176.2.367](https://doi.org/10.1093/mnras/176.2.367)
- Majumdar, L., Gratier, P., Ruaud, M., et al. 2016, *MNRAS*, stw3360, doi: [10.1093/mnras/stw3360](https://doi.org/10.1093/mnras/stw3360)
- Markevitch, M., Gonzalez, A. H., Clowe, D., et al. 2004, *ApJ*, 606, 819, doi: [10.1086/383178](https://doi.org/10.1086/383178)
- McMahan, A. K., Beck, H., & Krumhansl, J. A. 1974, *PhRvA*, 9, 1852, doi: [10.1103/PhysRevA.9.1852](https://doi.org/10.1103/PhysRevA.9.1852)
- Mo, H., van den Bosch, F. C., & White, S. 2010, *Galaxy Formation and Evolution* (Cambridge New York: Cambridge University Press). <https://ui.adsabs.harvard.edu/abs/2010gfe..book.....M>

- Ohmura, T., & Ohmura, H. 1960, *Physical Review*, 118, 154, doi: [10.1103/physrev.118.154](https://doi.org/10.1103/physrev.118.154)
- ONeil, S. V., & Reinhardt, W. P. 1978, *JChPh*, 69, 2126, doi: [10.1063/1.436813](https://doi.org/10.1063/1.436813)
- Pachucki, K. 2010, *PhRvA*, 82, 032509, doi: [10.1103/PhysRevA.82.032509](https://doi.org/10.1103/PhysRevA.82.032509)
- Pequignot, D., Petitjean, P., & Boisson, C. 1991, *A&A*, 251, 680
- Poll, J. D., & Wolniewicz, L. 1978, *JChPh*, 68, 3053, doi: [10.1063/1.436171](https://doi.org/10.1063/1.436171)
- Poszwa, A., Bahar, M. K., & Soyly, A. 2016, *Physics of Plasmas*, 23, 103515, doi: [10.1063/1.4965909](https://doi.org/10.1063/1.4965909)
- Rees, M. J. 1976, *MNRAS*, 176, 483, doi: [10.1093/mnras/176.3.483](https://doi.org/10.1093/mnras/176.3.483)
- Rosen, N. 1931, *Physical Review*, 38, 2099, doi: [10.1103/physrev.38.2099](https://doi.org/10.1103/physrev.38.2099)
- Rosenberg, E., & Fan, J. 2017, *PhRvD*, 96, doi: [10.1103/physrevd.96.123001](https://doi.org/10.1103/physrevd.96.123001)
- Ryan, M., & Shandera, S. 2021, In preparation
- Sakurai, J. J., & Napolitano, J. 2017, *Modern Quantum Mechanics* (Cambridge University Press), doi: [10.1017/9781108499996](https://doi.org/10.1017/9781108499996)
- Savin, D. W., Krsti, P. S., Haiman, Z., & Stancil, P. C. 2004, *ApJ*, 606, L167, doi: [10.1086/421108](https://doi.org/10.1086/421108)
- Shandera, S., Jeong, D., & Gebhardt, H. S. G. 2018, *PhRvL*, 120, doi: [10.1103/physrevlett.120.241102](https://doi.org/10.1103/physrevlett.120.241102)
- Silvera, I. F. 1980, *Reviews of Modern Physics*, 52, 393, doi: [10.1103/RevModPhys.52.393](https://doi.org/10.1103/RevModPhys.52.393)
- Sims, J. S., & Hagstrom, S. A. 2006, *JChPh*, 124, 094101, doi: [10.1063/1.2173250](https://doi.org/10.1063/1.2173250)
- Singh, D., Ryan, M., Magee, R., et al. 2020, arXiv e-prints, arXiv:2009.05209. <https://arxiv.org/abs/2009.05209>
- Stancil, P. C., Babb, J. F., & Dalgarno, A. 1993, *ApJ*, 414, 672, doi: [10.1086/173113](https://doi.org/10.1086/173113)
- Stancil, P. C., Lepp, S., & Dalgarno, A. 1998, *ApJ*, 509, 1, doi: [10.1086/306473](https://doi.org/10.1086/306473)
- Takayanagi, K., & Nishimura, S. 1960, *Publications of the Astronomical Society of Japan*, 12, 77
- Turner, J., Kirby-Docken, K., & Dalgarno, A. 1977, *ApJS*, 35, 281, doi: [10.1086/190481](https://doi.org/10.1086/190481)
- Walker, K. M., Yang, B. H., Stancil, P. C., Balakrishnan, N., & Forrey, R. C. 2014, *ApJ*, 790, 96, doi: [10.1088/0004-637x/790/2/96](https://doi.org/10.1088/0004-637x/790/2/96)
- Wang, J. G., & Stancil, P. C. 2002, *PhyS*, T96, 72, doi: [10.1238/physica.topical.096a00072](https://doi.org/10.1238/physica.topical.096a00072)
- Wrathmall, S. A., & Flower, D. R. 2007, *Journal of Physics B Atomic Molecular Physics*, 40, 3221, doi: [10.1088/0953-4075/40/16/003](https://doi.org/10.1088/0953-4075/40/16/003)
- Zhang, D., & Willitsch, S. 2018, in *Cold Chemistry: Molecular Scattering and Reactivity Near Absolute Zero* (The Royal Society of Chemistry), 496–536, doi: [10.1039/9781782626800-00496](https://doi.org/10.1039/9781782626800-00496)